
Constraints on the source of reactive phases in sediment from a major Arctic river using neodymium isotopes

Larkin Christina S. ^{1,*}, Piotrowski Alexander M. ¹, Hindshaw Ruth S. ¹, Bayon Germain ², Hilton Robert G. ³, Baronas J. Jotautas ¹, Dellinger Mathieu ³, Wang Ruixue ¹, Tipper Edward T. ¹

¹ Univ Cambridge, Dept Earth Sci, Cambridge, England.

² IFREMER, Marine Geosci Unit, Brest, France.

³ Univ Durham, Dept Geog, Durham, England.

* Corresponding author : Christina S. Larkin, email address : csl42@cam.ac.uk

Abstract :

Riverine suspended particulate matter (SPM) is essential for the delivery of micronutrients such as iron (Fe) to the oceans. SPM is known to consist of multiple phases with differing reactivity, but their role in the delivery of elements to the oceans is poorly constrained. Here we provide new constraints on the source and composition of reactive phases in SPM from the Mackenzie River, the largest sediment source to the Arctic Ocean. Sequential leaching of SPM shows that river sediments contain labile Fe phases. We estimate the labile Fe flux is substantial (0.21(+0.06,-0.05) Tg/yr) by quantifying Fe concentrations in weak leaches of the SPM. The labile Fe phase hosts a considerable amount of rare earth elements (REE), including neodymium (Nd). We demonstrate that the labile Fe phase and dissolved load have radiogenic Nd isotope ratios that are identical within uncertainty, but up to 8 epsilon units distinct from the silicate phase. We interpret this as evidence for dynamic cycling between Fe-oxide phases in SPM and the river water, demonstrating the high reactivity of the labile Fe phase. Nd isotope and elemental molar ratios suggest that a significant amount of labile Fe- and Nd-bearing phases are derived from Fe-oxides within the sedimentary source rock rather than silicate mineral dissolution. Thus, sedimentary rock erosion and weathering provides an important source of labile Fe, manganese (Mn) and by extension potentially other trace metals. Our results imply that both past and future environmental change in the Arctic, such as permafrost thaw, may trigger changes to the supply of reactive trace metals. These results demonstrate that a re-evaluation of sediment reactivity within rivers is required where uplifted sedimentary rocks are present.

Highlights

► Assessment of reactive phases in suspended particulates in a major Arctic river. ► Neodymium isotopes show equilibration between Fe-Mn oxides and dissolved loads. ► Reactive iron flux from the Mackenzie River is large; $0.21(+0.06,-0.05)$ Tg/yr. ► Sedimentary rock weathering provides an important source of labile trace metals.

Keywords : iron oxides, bioavailable, neodymium isotopes, Arctic

51

52 **1. Introduction**

53

54 Rivers are conduits for the transfer of particulate and dissolved material derived from
55 weathering to the oceans (Gaillardet et al., 1999). Weathering plays a critical role in
56 the cycling of elements at the Earth's surface and is a key regulator of the Earth's
57 climate over geological timescales (Walker et al., 1981). Rivers also transport
58 essential nutrients to the oceans sustaining marine primary productivity (e.g.,
59 Deutsch and Weber, 2012). Changes to the flux of nutrients that limit productivity in
60 the oceans have been linked to large scale perturbations in the carbon cycle and
61 past climate change (Martin, 1990; Vincent and Berger, 1985). The flux of
62 suspended particulate matter (SPM) sustains the supply of certain elements to the
63 oceans and plays an important role in bio-geochemical cycling (Jeandel and Oelkers,
64 2015; Jones et al., 2012).

65

66 Micronutrients (e.g., Fe), the rare earth elements (REE, particularly Nd) and many
67 other trace elements have low solubility in natural waters. In the dissolved load (<0.2
68 μm) these elements are predominately associated with nanoparticulate and colloidal
69 phases (Gaillardet et al., 2014, and references therein). Their concentrations in river
70 dissolved loads are low (ppb to ppt, Gaillardet et al., 2014); concentrations in SPM
71 are several orders of magnitude higher (Jeandel and Oelkers, 2015). Salt-induced
72 flocculation of many such nonmobile elements in estuaries further removes most of
73 these low concentration elements prior to reaching the oceans (Elderfield et al.,
74 1990).

75

76 Basalts and volcanic particulates are important sources of key bio-limiting nutrients
77 (e.g. Fe) as they are easily weatherable and enriched in those elements (Jones et
78 al., 2012). However, the importance of sedimentary rocks has not been similarly
79 evaluated. Marine sediments contain phases, including Fe-Mn oxyhydroxides with
80 elevated REE concentrations, which are formed from precipitation and exchange
81 with seawater and pore fluids (e.g., Chester and Hughes, 1967). Marine sedimentary
82 rocks tectonically emplaced on the continents retain some of these characteristics
83 (Hindshaw et al., 2018; Jang et al., 2020). This results in a reservoir of inherited
84 phases which can be more reactive than silicate minerals and may supply a greater
85 amount of bioavailable Fe to riverine sediments (Hindshaw et al., 2018). For
86 instance, amorphous Fe (oxy)hydroxides (e.g. ferrihyrite) contained within riverine
87 sediments are easily reducible and potentially bioavailable (Bhatia et al., 2013,
88 Hawkings et al., 2018).

89
90 Since Fe-oxides are enriched in REEs, their origin can be traced using radiogenic Nd
91 isotopes ($^{143}\text{Nd}/^{144}\text{Nd}$, expressed as ϵNd), a source tracer in riverine and marine
92 sediments (Goldstein and Jacobsen, 1988; Goldstein and Hemming, 2003). Since
93 there is limited fractionation of the Sm/Nd ratio in particulate phases during
94 weathering and the decay constant is long compared to the timescales of recent
95 weathering (Babechuk et al., 2014), ϵNd is only controlled by changes in source. Nd
96 in the dissolved load typically has ϵNd greater (more radiogenic) than in the SPM in
97 rivers with abundant sedimentary rocks in their catchments (Goldstein and
98 Jacobsen, 1987; Hindshaw et al., 2018). This offset is attributed to dissolved Nd
99 sourced from the preferential weathering of marine precipitates and other reactive
100 components contained within the parent rock (Goldstein and Jacobsen, 1987).

101 Nonetheless, a clear link between these reactive phases and dissolved riverine
102 chemistry has not been shown.

103

104 With knowledge of the source composition, ϵNd is a valuable tool for tracing the
105 origin of reactive phases from sedimentary rock weathering and their transport in
106 river systems. We apply this tracer to a large Arctic river system. The Mackenzie
107 River, as the first and third largest source of suspended sediment and water,
108 respectively, to the Arctic Ocean (Macdonald et al., 1998, Holmes et al., 2002),
109 provides a good representation of basin-scale fluxes. It is dominated by shale
110 weathering with a low abundance of volcanic or mafic rocks and limited influence
111 from the weathering of crystalline rocks (Millot et al., 2003, Fig. 1B). This makes the
112 Mackenzie an ideal location to investigate the mobilisation of reactive, micronutrient-
113 bearing phases during shale weathering on a large scale.

114

115 In this study we characterize the ϵNd of the dissolved load ($<0.2\ \mu\text{m}$ and
116 ultrafiltrates) and suspended sediment (sequential extractions and residue) in the
117 Mackenzie and key tributaries over two years (2017, 2018) sampled within a few
118 days of the peak discharge after ice-break up. We show that the ϵNd is within
119 uncertainty between the dissolved load and easily leachable phases in the SPM. We
120 use REE patterns to constrain the mineralogy of the leachable phases. We quantify
121 the concentrations of major and some trace elements in leachable phases and
122 estimate the flux of labile Fe from the Mackenzie to the Arctic Ocean.

123

124 **2. Materials and Methods**

125

126 Full analytical and procedural methods are given in Supplementary Text 1 and
127 summarised briefly here. All analysis was carried out at the University of Cambridge,
128 Department of Earth Sciences.

129

130 **2.1 Study area and sample collection**

131

132 The Mackenzie River system is large (Fig. 1, area 1.78×10^6 km²). The weathering of
133 sedimentary rocks dominates the dissolved and SPM loads of the river (Calmels et
134 al., 2007; Horan et al., 2019; Huh et al., 2004; Millot et al., 2003) despite the large
135 surface area of crystalline rocks (29.2% of the basin geology, Fig. 1b). Less than 1%
136 of the basin is underlain by volcanic rocks (Fig. 1b). The river is characterised by a
137 sharp peak in discharge each year after the seasonal melting (freshet) of river ice in
138 May-July (Fig. 2). Samples were collected at this period of maximum flux.

139

140 The Mackenzie mainstem and two large tributaries which enter at the delta, the Peel
141 River and the Arctic Red River, were sampled at 3 main sites (Fig. 1) in early June in
142 2017 and 2018. Suspended sediment samples were taken at different depths in the
143 channel using a 5L Van-Dorn type depth sampler (following Hilton et al., 2015).

144 Discharge was quantified using an acoustic-Doppler current profiler (ADCP, Rio
145 Grande II (1200 kHz), Teledyne Instruments, Fig. 2, Supplementary Table S4).

146 Additionally, in 2018 a small Peel River tributary and meltwater from the surface
147 Arctic Ocean (seawater diluted by sea and river ice melt) were sampled. Dredged
148 bed load, bank sand and rock fragments were also collected.

149

150 River samples were filtered at 0.2 μm , collecting both water and sediment. Filtered
151 waters collected for major cation and REE concentrations were acidified using
152 distilled HNO_3 to pH 2 in acid cleaned bottles. In 2018, ultrafiltration was carried out
153 on $<0.2 \mu\text{m}$ filtrates from the Mackenzie (Middle Channel) and the Peel River, using
154 dialysis membranes with molecular cut off weights of 10 kDa and 1 kDa
155 (Supplementary Text 1.2). Approximately 10 L of $<0.2 \mu\text{m}$ water was collected for the
156 analysis of Nd isotopes using a Fe co-precipitation method (Hindshaw et al., 2018).

157

158 To characterize the longer-term integrated composition of the Mackenzie River SPM
159 leachate compositions from 5 offshore sediment cores from the Mackenzie delta and
160 one from deeper in the Beaufort Sea were analysed (Natural Resources Canada,
161 Geology Survey of Canada's Marine Geoscience Collection, Supplementary Table
162 S5). Two silicate residue samples were analysed from two of the shallowest core
163 sites. The sedimentation rate at shallow sites in the Canadian Beaufort sea is high
164 (on the order of 2-3 m/ka, O'Regan et al., 2018), indicating that the range and depth
165 sampled within the cores (~ 10 cm) represents sediment that is likely several
166 decades old, and homogenises inter-annual and seasonal variability.

167

168 **2.2 Sequential extractions**

169

170 Approximately 50-100 mg of dry sediment was leached sequentially to extract: 1)
171 exchangeable phases (1M NH_4Cl), 2) reactive Fe-Mn (oxy)hydroxides (a weak acid-
172 reductive leach of 5 mM hydroxylamine hydrochloride (HH)-3 mM Na-EDTA-1.5%
173 acetic acid buffered to a pH of ~ 4 with NaOH), 3) calcite and additional carbonates
174 (1.7M acetic acid), 4) dolomite, and any remaining authigenic components (e.g.,

175 crystalline Fe-Mn oxides, 1M HCl). The focus of this study is the weak acid-reductive
176 leach, hereafter referred to as the HH leach, targeting amorphous reactive Fe-Mn
177 oxides. This is a more dilute HH leach than previous methods (e.g. Bhatia et al.,
178 2013; Chester and Hughes, 1967) carried out on non-decarbonated sediments,
179 following Blaser et al., 2016. This method minimizes dissolution of silicate phases
180 and avoids the loss of other reactive Fe phases during removal of carbonates. Due
181 to the buffering of this reaction in the presence of varying amounts of carbonate, it
182 represents a minimum estimate of the reactive Fe-Mn oxyhydroxides rather than a
183 fully quantitative leach. This leach will mobilise reactive carbonate phases and
184 potentially some REEs associated with phosphates. Residue sediment was digested
185 following lithium borate fusion (Supplementary Text S1.3).

186

187 **2.3 Major and trace concentration analysis**

188

189 Major and selected trace element (e.g. Fe, Mn) concentrations on acidified waters
190 were determined by ICP-OES (Agilent 5100, with a precision and accuracy of better
191 than 10% based on repeated analysis of certified water standards (Supplementary
192 Text 1.4.1).

193

194 Leachate phases and dissolved sediment residues were similarly analysed for major
195 and some trace element concentrations by ICP-OES, with matrix-matched calibration
196 lines. External reproducibility (typically better than 10%) was monitored using
197 certified standards (Supplementary Text 1.4.1).

198

199 Mass balance was verified by comparison of the sum of concentrations in the
200 leachates and residue with bulk sediment and a leached USGS shale standard with
201 certified values (Supplementary Table 8). The sum reproduced expected values
202 usually within 10%, and always within 20%.

203

204 **2.4 REE Analysis**

205

206 REE concentrations on filtered waters were measured by isotope dilution
207 (Supplementary Text 1.5). Nd (alongside REE) concentrations in sediments and
208 sediment leachates were determined using ICP-OES (Agilent 5100, Nd
209 concentrations > ~4 ppb only) and using a Thermo Element-XR ICP-MS with a
210 matrix-matched calibration line. Reproducibility was monitored using certified
211 standards and values were within $\pm 10\%$. Two residue samples and all sequential
212 extraction steps from one SPM sample were determined by isotope dilution, as
213 described for filtered water samples (Supplementary Text 1.5).

214

215 **2.5 Nd and Sr isotopes**

216

217 Nd was separated from the leachate and residue solutions using established
218 chromatographic procedures; the light REE's were separated using TRUspec resin,
219 and Nd from Sm using LNspec resin. Radiogenic Sr isotope ratios ($^{87}\text{Sr}/^{86}\text{Sr}$) were
220 determined on a subset of water, sediment leachate and sediment samples. Sr was
221 isolated using SrSpec resin (following Hindshaw et al, 2018). Nd was separated from
222 water samples using two stages of cation exchange (Biorad AG50W-X8) and
223 LnSpec resin (Supplementary Text 1.1).

224

225 Nd and Sr isotopes were measured on a Thermo Neptune Plus MC-ICP-MS.

226 $^{146}\text{Nd}/^{144}\text{Nd}$ was normalised to 0.7219 using an exponential correction. Samples

227 were corrected to the accepted value of reference standard JNdi-1;

228 $^{143}\text{Nd}/^{144}\text{Nd}=0.512115$ (Tanaka et al., 2000) which was repeatedly analysed at the

229 sample concentration throughout each measurement session. Two times the

230 standard deviation (2σ) on JNdi-1 for each measurement session is quoted as the

231 analytical uncertainty. ϵNd was calculated in parts per 10,000 relative to the

232 chondritic uniform reservoir (CHUR), $^{143}\text{Nd}/^{144}\text{Nd}_{\text{CHUR}}=0.512638$ (Jacobsen and

233 Wasserburg, 1980). For Nd isotopes, long-term reproducibility was monitored using

234 rock standards (Supplementary Text 1.4.2). Unless otherwise stated, where Nd

235 isotope replicates (measurement or full procedural) were carried out, the value

236 reported is the average of the replicates and the associated 2σ , if higher than the

237 measurement session uncertainty. For Sr isotopes, ^{85}Rb was monitored to correct for

238 Rb interferences on ^{87}Sr and Kr interferences were corrected for by measurement of

239 the baseline in a blank solution (on-peak zeros). Values were normalised to $^{86}\text{Sr}/^{88}\text{Sr}$

240 = 0.1194 using an exponential correction. For Sr isotopes, samples were analysed in

241 duplicate, and the uncertainty quoted is the associated 2σ . Repeated measurements

242 of the standard NBS 987 yielded $^{87}\text{Sr}/^{86}\text{Sr}=0.710275\pm 46$ ppm (2σ , $n=20$).

243

244 **3. Results**

245

246 **3.1 Dissolved Nd**

247

248 Nd was partitioned between nano-particulate and colloidal phases and the 'truly'
249 dissolved (<1 nm; ≈1 kDa) phase (Table 1). Approximately 70% of Nd in the <0.2 μm
250 filtrate is hosted in colloids or nano-particulates (Table 1). In the Mackenzie River
251 (Middle Channel) εNd values between the <0.2 μm and <1 kDa fractions agreed
252 within 0.43 epsilon units (Table 1). This demonstrates that nano-particulate and
253 colloidal phases and the 'truly' dissolved load have the same source and so the <0.2
254 μm εNd value is representative of the 'truly' dissolved composition, consistent with
255 previous observations in large rivers (Merschel et al., 2017).

256

257 **3.2 Paired sediment and dissolved εNd**

258

259 As the <0.2 μm fraction is indicative of the 'truly' dissolved εNd, it is possible to use
260 these measurements to compare with leachable phases and assess their reactivity.
261 We therefore refer to the <0.2 μm as the dissolved load. The dissolved load is
262 always more radiogenic than the sediment residue, with the offset ranging from 1.4
263 to 8.2 epsilon units (Fig. 3, average = 3.2). This is consistent with, and in some
264 cases far exceeds, the offset observed by Goldstein and Jacobsen, 1987, for large
265 rivers with significant marine sedimentary source rocks in their catchments. In
266 contrast, εNd in the dissolved load is in close agreement with HH leachates targeting
267 reactive Fe-Mn oxides with a linear regression within error of the 1:1 line (Fig. 3).
268 The dissolved vs. residue εNd linear regression is systematically offset from the 1:1
269 line, with a weaker correlation (Fig. 3).

270

271 Residue εNd compositions are in close agreement with previous measurements of
272 sediment already reported for the Mackenzie River (Vonk et al., 2015). Dissolved

273 ϵNd reported herein for the Mackenzie River at Tsiigehtchic (-13.4 ± 0.2 (2σ , $n=1$,
274 2018) and -12.3 ± 0.3 (2σ , $n=2$, 2017)) is consistent with the only previous dissolved
275 measurement (2003, -12.9 ± 0.3 (Zimmermann et al., 2009)).

276

277 SPM in the Middle Channel of the Mackenzie River is hydrodynamically sorted, due
278 to faster settling velocities of coarser sedimentary particles (e.g. Bouchez et al.,
279 2011). This is illustrated by Al/Si, a proxy for grain size (Fig. 4), indicating the
280 dominance of finer sediments towards the surface and coarser at the bottom.

281 Despite this hydrodynamic sorting, there is no appreciable variation of ϵNd with
282 depth in either the sediment residue or HH leachate (Fig. 4). Dissolved ϵNd from the
283 surface and base of the water column demonstrate that the water is well mixed.

284

285 There are systematic differences in dissolved ϵNd between 2017 and 2018. The
286 furthest downstream site (Mackenzie, Middle Channel) dissolved composition
287 changes from $\epsilon\text{Nd} = -10.71 \pm 0.41$ (2σ , $n=3$, 2017) to -12.97 ± 0.15 (2σ , $n=1$, 2018),
288 likely driven by changes in the Peel River which shows similar differences, changing
289 from $\epsilon\text{Nd} = -9.83 \pm 0.16$ (2σ , $n=1$, 2017) to -11.47 ± 0.15 (2σ , $n=1$, 2018). This could
290 represent inter-annual ϵNd variability, as is argued to be the case for changes in
291 organic carbon and dissolved nutrient sources on the same sample set (Schwab et
292 al., 2020), but additional data would be needed to determine if this is the case.

293

294 The average HH leach ϵNd from sediment cores was -11.3 ± 1.9 (2σ , $n=6$), consistent
295 with the same fraction in riverine sediments (Fig. 3) with the leachate always more
296 radiogenic compared to the silicate residue (two cores, $<10\text{m}$ deep, average offset =
297 2.7 ± 1.2 , 2σ , $n=2$). Shallow ($<100\text{ m}$) seawater in the Beaufort Sea is more

298 radiogenic than these leachate compositions ($\epsilon\text{Nd} = \sim -6$ to -9 , Porcelli et al., 2009).
299 Therefore, the offset between residue and leachate is preserved and exported in
300 sediment to the shelf. ϵNd in the HH leachate at the deepest and least proximal core
301 site ($\epsilon\text{Nd} = -9.55$, 1054 m water depth) overlaps with ϵNd measured in deep (> 1000
302 m) seawater in the Beaufort Sea, which is less radiogenic (ϵNd between -9 and -11 ,
303 Porcelli et al., 2009).

304

305 **3.3 Sediment partitioning and characterisation**

306

307 The partitioning of selected elements amongst all leachates relative to the bulk
308 sediment is shown in Fig. 5. In the NH_4Cl leach, targeting exchangeable phases, Fe
309 and Nd were below detection. This is consistent with a previous study which reported
310 low concentrations of REEs in a river sediment exchangeable fraction (Adebayo et
311 al., 2018). Elemental concentrations in the NH_4Cl leach which were not below
312 detection are reported in Tipper et al., 2021. The HH leach contains on average 3%,
313 8% and 30% of the total sediment Fe, Nd and Mn respectively (Fig. 5). Ca, Mg and
314 Sr are also high in the HH leach (Fig. 5) consistent with significant carbonate
315 lithologies present within the Mackenzie Basin (Milot et al., 2003). On average 60%
316 of the Fe and Nd are hosted within the silicate residue.

317

318 REE on the HH leach show a middle REE (MREE) enrichment (Fig. 6a). A MREE
319 enrichment of this magnitude is typical of an Fe-Mn oxyhydroxide signature (Fig. 6a)
320 and is consistent with that previously reported for similar sediment extractions (e.g.
321 Leybourne and Johannesson, 2008).

322

323 REE in the SPM leachate phases were partitioned relative to the bulk (sum of
324 leachates and residue; Middle Channel, 2017, Fig 6b). 15% of REEs relative to the
325 total sediment are mobilised during the HH leaching step. A smaller fraction (<1%) of
326 REEs are released during the subsequent acetic acid leach step (Fig. 6b), despite
327 the large amount of Ca and Mg (22% of total sediment Ca, 11% of total sediment
328 Mg). Less Fe and Mn are mobilised in the acetic acid leach (1% of total Fe, 5% of
329 total Mn), relative to the HH leach (4% of total Fe, 42% of total Mn). This
330 demonstrates that the REE are not associated with carbonate phases.

331

332 $^{87}\text{Sr}/^{86}\text{Sr}$ on the dissolved load and sediment residues (Fig. 6c) are in agreement
333 with previously published data for this river (e.g. Millot et al., 2003). $^{87}\text{Sr}/^{86}\text{Sr}$ values
334 indicate carbonate and silicate sources in the HH leach and residue respectively. Sr
335 isotopes do not indicate extensive leaching into the silicate detrital fraction. Although
336 there is scatter in the leachable ϵNd compositions (Fig. 6c), on stronger leaching ϵNd
337 is not substantially more radiogenic than the HH leach.

338

339 **4. Discussion**

340

341 ϵNd values from paired dissolved load and SPM, alongside the characterisation of
342 elemental concentrations in sequential extractions, are used to trace both the source
343 and the reactivity of different phases within the SPM. Firstly, we seek to assess the
344 reactivity of the phases in the HH leach and then characterise sources. We then
345 estimate the flux of labile Fe from the Mackenzie to the Arctic Ocean and address
346 the implications of this study in terms of the oceanic Nd budget.

347

348 **4.1 Reactivity of the labile phases in SPM**

349

350 The reactivity of phases hosted in the HH leachate are traced with ϵNd and
351 elemental partitioning. Significant fractions of Fe, Mn, Ca, Mg, and REEs relative to
352 the bulk sediment are present in what is an extremely weak and buffered leach (5
353 mM HH, 1.5% acetic acid, Fig. 5, Fig. 6). Although subsequent leaches use stronger
354 reactants and are not buffered, they release smaller amounts of Nd compared to the
355 HH leach (Fig. 6b). This suggests that some of these reactive phases are
356 susceptible to acid-reductive dissolution with small changes in pH or redox
357 conditions (which may occur in the delta or offshore). Nd and REEs are depleted in
358 carbonate rocks and are unlikely to be directly incorporated into biogenic calcite (e.g.
359 Tachikawa et al., 2014). Less Nd is released in the 1.7 M acetic acid leach,
360 compared to the HH leach, confirming that during the HH leaching step the Nd
361 released is not associated with carbonates.

362

363 Although an MREE enrichment in the HH leach is typical of an Fe-Mn oxyhydroxide
364 phase, this could also be consistent with some phosphate phases (such as biogenic
365 apatite, Fig. 6a., Leybourne and Johannesson, 2008, and references therein).

366 Secondary precipitation of phosphates could also result in an MREE enrichment
367 (Leybourne and Johannesson, 2008), but the lack of an LREE enrichment (low
368 HREE/LREE, Fig. 6a) in HH leaches makes this unlikely (Köhler et al., 2005).

369

370 The dissolved ϵNd composition is always similar to the HH leachate composition
371 (Fig. 3). This similarity is prevalent in different sampling localities and tributaries,
372 which differ in sediment and water characteristics. This points to a fundamental

373 process that is shared between these catchments and suggests that this observation
374 is not unique to the time of year sampled (freshet). In rivers, the SPM is supplied by
375 bank erosion and hillslope processes (Hilton et al., 2015), which are likely to be
376 decoupled in space and time from the hydrological pathways that deliver river water
377 (Vonk et al., 2019). Therefore, the consistency in ϵNd between dissolved and HH
378 leach ϵNd is most likely explained by rapid and recent cycling within riverine implying
379 equilibrium between the dissolved load and Fe-oxide phases in the HH leach.

380

381 Dissolved and HH leachate ϵNd are always similar at each site in the Mackenzie
382 River, both upstream and downstream of major confluences with the Peel and Arctic
383 Red Rivers (Tsiigehtchic to Middle Channel, Fig. 1a). Previous discharge and
384 sediment flux estimates demonstrate that water and suspended sediment do not mix
385 in the same proportions downstream of the Peel confluence, with the Peel supplying
386 17% of the sediment load (Carson et al., 1998), but only 7% of the total water
387 discharge (Schwab et al., 2020 and references therein). This implies the potential for
388 rapid cycling between the dissolved load and HH leach phases during transit
389 between the upstream and downstream sites, despite only limited changes in pH and
390 Nd concentration (supplementary Table S4 and S10).

391

392 Although the mechanism for equilibration of Nd between HH leach phases and the
393 dissolved load is unclear, since the weakly adsorbed exchangeable phases are
394 removed in the leaching step prior to the HH leach, this rapid cycling is likely driven
395 by dissolution of Nd from phases such as Fe-Mn oxyhydroxides. The concentration
396 of Nd in the HH leach (ppb to ppm, Supplementary Table S9 and S11) is several
397 orders of magnitude higher than the dissolved concentration (Supplementary Table

398 S10), suggesting that phases within the HH leach may drive the dissolved
399 composition.

400

401 Our findings demonstrate dynamic cycling between the dissolved load and phases
402 soluble in the HH leach, such as Fe-Mn oxyhydroxides. The similarity of the
403 dissolved load and HH leach phases and decoupling from the silicate residue
404 suggests that the HH leach phases are labile and likely bioavailable. These results
405 imply not only rapid cycling of Nd but potentially other immobile elements contained
406 within the HH leach.

407

408 **4.2 Marine authigenic phases as a source of radiogenic Nd in river waters**

409

410 The mass balance of sources of radiogenic Nd that contribute to higher ϵNd in the
411 dissolved and HH fractions relative to silicates provides information on the relative
412 supply of Nd from different phases. Here we discuss possible sources of radiogenic
413 Nd that could explain both the HH leaches and dissolved load. Average global
414 seawater ϵNd (~ -8.8 , Lacan et al., 2012) and modern core top authigenic fractions
415 (Haley et al., 2017) are more radiogenic than the upper continental crust (-11.4 ± 2.5 ,
416 Goldstein et al., 1984). Therefore, when marine sediments are emplaced on the
417 continents, they can provide a distinct source of radiogenic Nd to the weathering
418 reactor. Measurements of ϵNd on Fe-Mn oxides and other inherited authigenic
419 phases of marine origin hosted in sedimentary rocks show that they are on average
420 more radiogenic than associated silicates (Jang et al., 2020, Hindshaw et al., 2018).
421 They can be reactive and so result in a more radiogenic dissolved and leachate

422 composition when compared to the bulk source rock in rivers (Bayon et al., 2020;
423 Goldstein and Jacobsen, 1987; Hindshaw et al., 2018; Jang et al., 2020).

424

425 Preferential weathering of inherited marine authigenic phases is the most likely
426 reason for decoupled ϵNd between dissolved and silicate residue sediment in the
427 Mackenzie. Radiogenic Nd in Fe-Mn oxyhydroxides of Mackenzie River SPM is likely
428 derived from the weathering of these phases through physical transportation, and
429 equilibration with waters. These radiogenic phases become mixed with Fe-oxides
430 resulting from the weathering of silicate minerals, with ϵNd inherited from the source
431 silicate. Nonetheless, it is possible that alternate sources contribute labile and
432 radiogenic Nd, and these are addressed below.

433

434 **4.3 Alternative sources of radiogenic Nd to river waters**

435 Accessory minerals enriched in REEs and garnet can have more radiogenic ϵNd
436 than their bulk source rocks (e.g. Rickli et al., 2017). However, radiogenic release of
437 Nd during incongruent weathering of crystalline rocks is minimal (Dausmann et al.,
438 2019). Another possible source of radiogenic Nd is the preferential weathering of
439 volcanic rocks, but they are rare in the Mackenzie basin (Fig 1b, Millot et al., 2003).

440

441 Several studies indicate the dominance of shale and carbonate weathering on the
442 Mackenzie dissolved load, with no evidence of large volcanic or crystalline rock
443 contributions (Horan et al., 2019; Huh et al., 2004; Millot et al., 2003). ϵNd
444 decoupling between dissolved and silicate residue is at a maximum in a small Peel
445 River tributary that, to the best of our knowledge, does not have crystalline or
446 volcanic rocks in its catchment and drains almost exclusively shales. Moreover,

447 preferential weathering of a specific rock type would not explain the coupling of the
448 dissolved load with the HH leach, and their decoupling from the silicate residue, in all
449 sampling sites, with differing source lithologies.

450 Phosphates in sedimentary rocks are enriched in REEs and may be partially
451 mobilised in the HH leach. Phosphates in the main source rock type (shales) are
452 likely to have formed during marine diagenesis, so can be considered as inherited
453 authigenic phases, with a comparable ϵNd to concurrent Fe-Mn oxides. Fe-oxides
454 are ubiquitous in all sediments and sedimentary rocks. Given the range in source
455 rock age (Proterozoic to Cenozoic, Wheeler, 1996) and depositional environment,
456 Fe-Mn oxides are the most probable universal constituent consistent with the high
457 fraction of Fe and Mn in the HH leach, whereas phosphates may not always be
458 present in sufficient abundance. Equilibration between the dissolved load and
459 phosphates hosted in the HH leach would not likely result in the observed REE
460 patterns, as secondary phosphates are typically LREE enriched (Fig. 6a, Köhler et
461 al., 2005). Therefore, it is unlikely that phosphate minerals play a significant role, and
462 the more positive Nd is derived from the preferential weathering of inherited Fe-Mn
463 oxides.

464

465 While Fe-Mn oxides are insoluble in oxygenated and neutral range pH which typify
466 large rivers including the Mackenzie (Tank et al., 2016) mobilization of amorphous
467 and nano-particulate Fe can occur, and in acidic environments dissolution of Fe-
468 oxides may occur. Extensive pyrite oxidation provides the majority of dissolved
469 sulfate in the Mackenzie (Calmels et al., 2007). A product of the oxidative weathering
470 of pyrite is Fe-oxide, and if instantaneous buffering of this reaction by dissolution of
471 carbonate minerals does not occur, it will result in an acidic pH alongside high sulfate

472 concentrations (Horan et al., 2019). This is seen in one tributary of the Peel River
473 where high sulfate concentrations (4660 μM) and relatively low pH of ~ 6 are coupled
474 to elevated Nd (950 ppt), high Fe (1 μM) and Mn (7.8 μM) concentrations in the
475 dissolved load ($<0.2 \mu\text{m}$, Supplementary Tables S9 and S12) with the highest
476 observed offset between the residue and HH leach ϵNd (8 epsilon units,
477 Supplementary Table S10).

478

479 Nd is not likely to be incorporated directly into pyrite but will be present in
480 'contaminant' phases in pyrite or in other phases within a sedimentary rock
481 succession, namely Fe-Mn oxyhydroxides or phosphates (Raiswell and Plant, 1980).
482 High Nd and Mn dissolved concentrations indicate the dissolution of reactive Fe-Mn
483 oxides within the source rock (shale), with differing ϵNd to silicate sources, coupled
484 to the oxidative weathering of pyrite.

485

486 The HH leach of a shale fragment from this catchment has comparable ϵNd to the
487 bedload HH leachate and dissolved load (Fig. 3, Supplementary Table S10).

488 Although the mineralogical source of Nd and Fe is different (Fe from pyrite and Nd
489 from other phases) these observations imply that the mobilization of Fe and Nd are
490 coupled during the oxidative weathering of pyrite. This suggests that oxidative
491 weathering of pyrite may provide an important source of reactive Nd and Fe bearing
492 phases, with radiogenic ϵNd . Once the REEs are in solution, they can be
493 incorporated into secondary Fe-oxides upon increasing pH, when Fe-oxides bearing
494 REEs will precipitate out of solution. Close coupling between riverine Nd and Fe has
495 been noted in previous studies (e.g. Elderfield et al., 1990; Ingri et al., 2000).

496

497 4.4 Constraints on the contribution of different sources of labile Fe and Nd

498

499 Using a simple mass balance model it is possible to estimate the fraction of Nd and
500 Fe sourced from inherited authigenic phases contained within the sedimentary
501 source rocks.

502

503 Dissolved ϵNd is set by exchange with labile HH leach phases in the SPM. The labile
504 ϵNd is considered to be a mixture of Fe-oxides derived from modern-day weathering
505 of silicate minerals ($\epsilon\text{Nd}_{\text{sil}}$) and Nd derived from inherited authigenic phases ($\epsilon\text{Nd}_{\text{auth}}$,
506 equation 1, Figure 7).

$$507 \quad \epsilon\text{Nd}_{\text{labile}} = f_{\text{Nd,auth}} \epsilon\text{Nd}_{\text{auth}} + f_{\text{Nd,sil}} \epsilon\text{Nd}_{\text{sil}} \quad (1)$$

508 where $\epsilon\text{Nd}_{\text{labile}}$ is the average of the leachate and dissolved composition, and f is the
509 fraction of Nd in either the inherited authigenic or silicate phases where $f_{\text{Nd,auth}} + f_{\text{Nd,sil}}$
510 = 1.

511

512 Equation 1 was solved for $f_{\text{Nd,auth}}$, with $\epsilon\text{Nd}_{\text{sil}}$ given by the residue silicate composition
513 measured for sample set. $\epsilon\text{Nd}_{\text{labile}}$ is the average of the HH leachate composition and
514 (if measured) the dissolved composition for each sample set. $\epsilon\text{Nd}_{\text{auth}}$ is unknown and
515 given the range of ages and types of sedimentary rocks in the Mackenzie basin, will
516 be variable. $\epsilon\text{Nd}_{\text{auth}}$ was considered over the range $\epsilon\text{Nd}_{\text{auth}}=0$ to $\epsilon\text{Nd}_{\text{auth}}= \epsilon\text{Nd}_{\text{labile}}$
517 sampled from a synthetic uniform distribution to account for the uncertainty of this
518 end-member. $\epsilon\text{Nd}_{\text{labile}}$ and $\epsilon\text{Nd}_{\text{sil}}$ were measured at each sampling location and
519 considered as normal distributions. We used Monte-Carlo methods to estimate the
520 error when solving for $f_{\text{Nd,auth}}$ (calculating $f_{\text{Nd,auth}}$ for 100,000 values of each variable).
521 $f_{\text{Nd,auth}}$ was calculated for 4 individual sample sets (2017 and 2018 Middle Channel,

522 Arctic Ocean and in shelf sediment cores, Fig. 8, Supplementary Table S13). Taking
523 the interquartile range from the sum of all four sample sets it estimated that, at the
524 mouth of the Mackenzie River a minimum of 23-50% of labile Nd is derived from
525 inherited authigenic phases (Fig. 8).

526

527 Given this significant estimate for $f_{Nd,auth}$, it is likely that a similarly high fraction of
528 other immobile elements such as Fe are also sourced from inherited authigenic
529 phases. The fraction of labile Fe sourced from inherited authigenic phases (including
530 from pyrite and inherited Fe-oxides) was estimated using mass balance:

531
$$\left(\frac{Nd}{Fe}\right)_{labile} = f_{Fe,sil} \left(\frac{Nd}{Fe}\right)_{sil} + f_{Fe,auth} \left(\frac{Nd}{Fe}\right)_{auth} \quad (2)$$

532 where $f_{Fe,auth} + f_{Fe,sil} = 1$, and $\left(\frac{Nd}{Fe}\right)_i$ is the molar ratio of Nd to Fe in each phase.

533 This equation was solved for $f_{Fe,auth}$, the fraction of labile Fe sourced from inherited
534 authigenic phases. $\left(\frac{Nd}{Fe}\right)_{auth}$ is unknown, and the largest source of error and was

535 based on the range from HH leaches of a shale fragment and coarse bank sediment

536 $\left(\left(\frac{Nd}{Fe}\right) \times 1000 = 0.63 \text{ to } 2.4\right)$. $\left(\frac{Nd}{Fe}\right)_{sil}$ was taken as the average of the measured

537 silicate residue values which are within error of average upper continental crustal

538 estimates $\left(\left(\frac{Nd}{Fe}\right) \times 1000 = 0.33 \pm 0.1\right)$, Supplementary Text 3). $\left(\frac{Nd}{Fe}\right)_{labile}$ is the measured

539 HH leachate composition at each sampling site. Using Monte Carlo methods to

540 estimate errors, $f_{Fe,auth}$ is estimated to be between 11-29% (interquartile range, from

541 sum of Middle Channel samples sets, 2017 and 2018, Supplementary Table S14).

542

543 Despite the uncertainty it is clear that the SPM in the Mackenzie must host a

544 significant fraction of labile Nd and Fe which is derived from inherited authigenic

545 phases in sedimentary rocks. Accordingly, the weathering of sedimentary rocks,
546 especially marine shales, must supply a significant amount of reactive immobile
547 elements (Nd, Fe) in the Mackenzie basin.

548

549 **4.5 The flux of labile, potentially bioavailable, Fe**

550

551 We have demonstrated that the SPM in the Mackenzie River has a labile Fe phase.
552 To estimate its supply to the Arctic Ocean, we use the suspended sediment flux,
553 which is well documented for the Mackenzie in the years 1974-1994. There is
554 significant inter-annual variability ranging from 81 Tg/yr to 224 Tg/yr (Carson et al.,
555 1998) with a consistent seasonal peak in the summer months following freshet, the
556 time period over which our samples were collected (Fig. 2).

557

558 The labile, potentially bioavailable, Fe concentration was considered to be equal to
559 the HH leach Fe concentration measured on SPM from the Mackenzie (Middle
560 Channel, 2017 and 2018), which approximated to a normal distribution (1466 ± 350
561 $\mu\text{g/g}$ ($\pm 1\sigma$, $n=16$)). The uncertainty was estimated using Monte-Carlo methods
562 ($n=100000$), similar to that used by Hilton et al., 2015. The sediment flux was
563 considered as a uniform distribution, taking into account all potential values at equal
564 probability (81 Tg/yr to 224 Tg/yr, Carson et al., 1998), a maximum approximation of
565 error. The median (\pm interquartile range) flux of labile Fe associated with SPM in the
566 Mackenzie River was calculated to be $0.21(+0.06,-0.05)$ Tg/yr. We do not include
567 dissolved ($<0.2 \mu\text{m}$) Fe concentrations in this estimate as they are negligible in
568 comparison to Fe hosted in the reactive sediment phase (estimated dissolved Fe flux
569 represents $<0.03\%$ of the labile sediment Fe flux, Supplementary Text 4).

570

571 The calculated flux of potentially bioavailable Fe in the SPM of the Mackenzie is
572 substantial; comparable to that from the Greenland Ice Sheet (~0.3 Tg/yr, Bhatia et
573 al., 2013). Greenland Ice Sheet fluxes are estimated using the sum of strong SPM
574 leaching and dissolved Fe followed by the application of an estuarine loss factor
575 (90%, Bhatia et al., 2013).

576

577 Much of the SPM from the Mackenzie is rapidly buried offshore or trapped in the
578 delta, and the loss due to estuarine processes is unknown. Even if ~90% of the
579 bioavailable Fe in the SPM is removed or trapped, the resulting flux to the oceans is
580 still significant (~0.02 Tg/yr). Moreover, benthic release of this particulate associated
581 Fe, alongside Nd, on the Mackenzie shelf may play an important role in delivering a
582 higher proportion of this labile phase to the Arctic Ocean.

583

584 For every two moles of sulfate released from the oxidative weathering of pyrite in the
585 Mackenzie basin, 1 mole of Fe will be incorporated into an Fe-oxide. Using the
586 pyrite-derived sulfate flux of Calmels et al., 2007 it is estimated that the oxidative
587 weathering of pyrite will result in the production of ~3.6 Tg/yr of Fe, as Fe-oxides.
588 This is around an order of magnitude greater than the labile Fe flux associated with
589 SPM that we estimate herein (0.2 Tg/yr). This implies a large accumulation of Fe-
590 oxides derived from the oxidative weathering of pyrite within the critical zone in the
591 Mackenzie basin, which are not exported to labile phases in the SPM.

592

593 **4.6 Nd isotopic end-member compositions and inputs to the Arctic ocean**

594

595 The Mackenzie River is a large point source of sediment and water to the Arctic
596 Ocean; therefore, it is an important finding that labile Nd has an isotopic composition
597 that is distinct from the bulk SPM. This finding is potentially applicable to all riverine
598 catchments with marine sedimentary source rocks. It is equally noteworthy that there
599 is variability in dissolved ϵNd between sampling years. Although our data is similar to
600 the only previous dissolved data point on the Mackenzie (Zimmermann et al., 2009),
601 it extends the range with implications for studies involving ϵNd in the Arctic Ocean
602 (e.g. Deschamps et al., 2019). Despite variability the HH leachates from shallow
603 marine core sites reflect the average dissolved composition of the Mackenzie over
604 decadal timescales. Therefore, such leachates from shelf sediment may provide a
605 more useful integrated ϵNd end-member. This isotopically distinct, labile, phase is
606 maintained offshore, meaning that any labelling of seawater via 'boundary exchange'
607 processes on the shelf will have a significantly more radiogenic composition than the
608 bulk sediment. This suggests that bulk shelf sediment and continental margin ϵNd
609 may be systematically offset from the likely oceanic source (Jeandel et al., 2007) as
610 it is the reactive (leachable) compositions which will characterise any shelf inputs.

611

612 **5 Conclusions**

613

614 This study highlights the potential for sedimentary rock weathering in the Arctic to
615 provide a critical source of labile Fe. As approximately half of the rocks weathered on
616 land draining into the Arctic Ocean are shales (Amiotte Suchet et al., 2003), similar
617 observations to this study would be expected in other Arctic rivers. The on-going
618 state of permafrost thaw in the Mackenzie basin has resulted in increased slumping
619 in the Peel catchment which has exposed fresh pyrite minerals and resulted in

620 increased sulfuric acid weathering (Zolkos et al., 2018). Increased exposure of pyrite
621 may also lead to increased mobility and dissolution of REEs (and Fe) within this
622 catchment. However, it is also important to note that delivery of bioavailable Fe from
623 the Mackenzie basin to the Arctic Ocean will have changed in the past, including
624 during periods of glaciation and glacial retreat in this region. Melt water and ice-
625 rafting could have allowed for more direct delivery of un-weathered labile Fe phases
626 to the Arctic Ocean.

627

628 Recycled sedimentary components within source rocks may provide labile
629 micronutrients and other trace elements, a process which is likely applicable globally,
630 and not just in the Arctic. Fe, and the supply of other micronutrients that limit primary
631 productivity, are thought to be capable of having long-term and far-reaching effects
632 on global climate, by way of their potential for increasing productivity and organic
633 carbon burial in the oceans. Therefore, when considering increases in nutrient
634 availability in the past, the source lithology and its reactivity must be taken into
635 consideration. We highlight the impact of source lithology on the budget of labile
636 trace elements (Nd) and micronutrients (Fe) in rivers, which has implications for both
637 present and past fluxes to the oceans and paves the way for restructuring how
638 riverine SPM is viewed in terms of its reactivity when sedimentary rocks are present
639 in the source catchment.

640

641 **Acknowledgements**

642

643 M. Greaves, G. Hughes, H. Chapman, M. Bickle and K. Relph are thanked for their
644 assistance in the lab. E. Amos and M. Schwab are thanked for assisting with

645 fieldwork. E. Stevenson is thanked for her help and advice on Arctic fieldwork and
646 the co-precipitation method. M. Murphy and C. Arendt are thanked for sharing their
647 methods for ultra-filtration and FeCl₃ cleaning respectively. Y. Plancherel and E.
648 Stevenson are thanked for supplying filtered Severn River water used as an internal
649 standard. K. Jarrett and the Geological Survey of Canada, Marine Geoscience
650 Collection are thanked for supplying sediment core subsamples. The authors both
651 thank and acknowledge the assistance of the Aurora College Research Institute,
652 Inuvik. Samples were collected under research licenses 15288 and 16106. C.S.L
653 was funded by a NERC studentship (NE/L002507/1) with support for travel to
654 Canada in 2018 from the University of Cambridge Department of Earth Sciences
655 Leave to Work Away Research Fund. R.G.H acknowledges funding from the
656 European Research Council (Starting Grant ROC-CO₂, 678779) and a NERC UK-
657 Canada Arctic Partnership Bursaries Program. E.T.T acknowledges funding from
658 NERC Standard Grant 703 NE/P011659/1. The manuscript was greatly improved by
659 comments from two helpful anonymous reviewers and the editor L. Derry.

660

661 **References**

- 662 Adebayo, S.B., Cui, M., Hong, T., White, C.D., Martin, E.E., Johannesson, K.H.,
663 2018. Rare Earth Elements Geochemistry and Nd Isotopes in the Mississippi
664 River and Gulf of Mexico Mixing Zone. *Front. Mar. Sci.* 5.
665 <https://doi.org/10.3389/fmars.2018.00166>
- 666 Amiotte Suchet, P., Probst, J.-L., Ludwig, W., 2003. Worldwide distribution of
667 continental rock lithology: Implications for the atmospheric/soil CO₂ uptake by
668 continental weathering and alkalinity river transport to the oceans. *Glob.*
669 *Biogeochem. Cycles* 17. <https://doi.org/10.1029/2002GB001891>

670 Babechuk, M.G., Widdowson, M., Kamber, B.S., 2014. Quantifying chemical
671 weathering intensity and trace element release from two contrasting basalt
672 profiles, Deccan Traps, India. *Chem. Geol.* 363, 56–75.
673 <https://doi.org/10.1016/j.chemgeo.2013.10.027>

674 Bayon, G., Lambert, T., Vigier, N., De Deckker, P., Freslon, N., Jang, K., Larkin,
675 C.S., Piotrowski, A.M., Tachikawa, K., Thollon, M., Tipper, E.T., 2020. Rare
676 earth element and neodymium isotope tracing of sedimentary rock
677 weathering. *Chem. Geol.* 119794.
678 <https://doi.org/10.1016/j.chemgeo.2020.119794>

679 Bhatia, M.P., Kujawinski, E.B., Das, S.B., Breier, C.F., Henderson, P.B., Charette,
680 M.A., 2013. Greenland meltwater as a significant and potentially bioavailable
681 source of iron to the ocean. *Nat. Geosci.* 6, 274–278.
682 <https://doi.org/10.1038/ngeo1746>

683 Blaser, P., Lippold, J., Gutjahr, M., Frank, N., Link, J.M., Frank, M., 2016. Extracting
684 foraminiferal seawater Nd isotope signatures from bulk deep sea sediment by
685 chemical leaching. *Chem. Geol.* 439, 189–204.
686 <https://doi.org/10.1016/j.chemgeo.2016.06.024>

687 Bouchez, J., Gaillardet, J., France- Lanord, C., Maurice, L., Dutra- Maia, P., 2011.
688 Grain size control of river suspended sediment geochemistry: Clues from
689 Amazon River depth profiles. *Geochem. Geophys. Geosystems* 12.
690 <https://doi.org/10.1029/2010GC003380>

691 Calmels, D., Gaillardet, J., Brenot, A., France-Lanord, C., 2007. Sustained sulfide
692 oxidation by physical erosion processes in the Mackenzie River basin:
693 Climatic perspectives. *Geology* 35, 1003. <https://doi.org/10.1130/G24132A.1>

694 Carson, M.A., Jasper, J.N., Conly, F.M., 1998. Magnitude and Sources of Sediment
695 Input to the Mackenzie Delta, Northwest Territories, 1974–94. *Arctic* 51, 116–
696 124. <https://doi.org/10.14430/arctic1053>

697 Chester, R., Hughes, M.J., 1967. A chemical technique for the separation of ferro-
698 manganese minerals, carbonate minerals and adsorbed trace elements from
699 pelagic sediments. *Chem. Geol.* 2, 249–262. <https://doi.org/10.1016/0009->
700 2541(67)90025-3

701 Dausmann, V., Gutjahr, M., Frank, M., Kouzmanov, K., Schaltegger, U., 2019.
702 Experimental evidence for mineral-controlled release of radiogenic Nd, Hf and
703 Pb isotopes from granitic rocks during progressive chemical weathering.
704 *Chem. Geol.* 507, 64–84. <https://doi.org/10.1016/j.chemgeo.2018.12.024>

705 Deschamps, C.-E., Montero- Serrano, J.-C., St- Onge, G., Poirier, A., 2019.
706 Holocene Changes in Deep Water Circulation Inferred From Authigenic Nd
707 and Hf Isotopes in Sediment Records From the Chukchi-Alaskan and
708 Canadian Beaufort Margins. *Paleoceanogr. Paleoclimatology* 34, 1038–1056.
709 <https://doi.org/10.1029/2018PA003485>

710 Deutsch, C., Weber, T., 2012. Nutrient Ratios as a Tracer and Driver of Ocean
711 Biogeochemistry. *Annu. Rev. Mar. Sci.* 4, 113–141.
712 <https://doi.org/10.1146/annurev-marine-120709-142821>

713 Elderfield, H., Upstill-Goddard, R., Sholkovitz, E.R., 1990. The rare earth elements in
714 rivers, estuaries, and coastal seas and their significance to the composition of
715 ocean waters. *Geochim. Cosmochim. Acta* 54, 971–991.
716 [https://doi.org/10.1016/0016-7037\(90\)90432-K](https://doi.org/10.1016/0016-7037(90)90432-K)

717 Gaillardet, J., Dupré, B., Louvat, P., Allègre, C.J., 1999. Global silicate weathering
718 and CO₂ consumption rates deduced from the chemistry of large rivers.
719 Chem. Geol. 159, 3–30. [https://doi.org/10.1016/S0009-2541\(99\)00031-5](https://doi.org/10.1016/S0009-2541(99)00031-5)

720 Gaillardet, J., Viers, J., Dupré, B., 2014. 7.7 - Trace Elements in River Waters, in:
721 Holland, H.D., Turekian, K.K. (Eds.), Treatise on Geochemistry (Second
722 Edition). Elsevier, Oxford, pp. 195–235. [https://doi.org/10.1016/B978-0-08-](https://doi.org/10.1016/B978-0-08-095975-7.00507-6)
723 [095975-7.00507-6](https://doi.org/10.1016/B978-0-08-095975-7.00507-6)

724 Goldstein, S.J., Jacobsen, S.B., 1988. Nd and Sr isotopic systematics of river water
725 suspended material: implications for crustal evolution. Earth Planet. Sci. Lett.
726 87, 249–265. [https://doi.org/10.1016/0012-821X\(88\)90013-1](https://doi.org/10.1016/0012-821X(88)90013-1)

727 Goldstein, S.J., Jacobsen, S.B., 1987. The Nd and Sr isotopic systematics of river-
728 water dissolved material: Implications for the sources of Nd and Sr in
729 seawater. Chem. Geol. Isot. Geosci. Sect. 66, 245–272.
730 [https://doi.org/10.1016/0168-9622\(87\)90045-5](https://doi.org/10.1016/0168-9622(87)90045-5)

731 Goldstein, S.L., Hemming, S.R., 2003. Long-lived isotopic tracers in oceanography,
732 paleoceanography, and ice-sheet dynamics. Treatise Geochem. 6, 453–489.

733 Goldstein, S.L., O’Nions, R.K., Hamilton, P.J., 1984. A Sm-Nd isotopic study of
734 atmospheric dusts and particulates from major river systems. Earth Planet.
735 Sci. Lett. 70, 221–236. [https://doi.org/10.1016/0012-821X\(84\)90007-4](https://doi.org/10.1016/0012-821X(84)90007-4)

736 Haley, B.A., Du, J., Abbott, A.N., McManus, J., 2017. The Impact of Benthic
737 Processes on Rare Earth Element and Neodymium Isotope Distributions in
738 the Oceans. Front. Mar. Sci. 4. <https://doi.org/10.3389/fmars.2017.00426>

739 Hawkings, J.R., Benning, L.G., Raiswell, R., Kaulich, B., Araki, T., Abyaneh, M.,
740 Stockdale, A., Koch-Müller, M., Wadham, J.L., Tranter, M., 2018. Biolabile

741 ferrous iron bearing nanoparticles in glacial sediments. *Earth Planet. Sci. Lett.*
742 493, 92–101. <https://doi.org/10.1016/j.epsl.2018.04.022>

743 Hilton, R.G., Galy, V., Gaillardet, J., Dellinger, M., Bryant, C., O'Regan, M., Gröcke,
744 D.R., Coxall, H., Bouchez, J., Calmels, D., 2015. Erosion of organic carbon in
745 the Arctic as a geological carbon dioxide sink. *Nature* 524, 84–87.
746 <https://doi.org/10.1038/nature14653>

747 Hindshaw, R.S., Aciego, S.M., Piotrowski, A.M., Tipper, E.T., 2018. Decoupling of
748 dissolved and bedrock neodymium isotopes during sedimentary cycling.
749 *Geochem. Perspect. Lett.* 43–46. <https://doi.org/10.7185/geochemlet.1828>

750 Holmes, R.M., McClelland, J.W., Peterson, B.J., Shiklomanov, I.A., Shiklomanov,
751 A.I., Zhulidov, A.V., Gordeev, V.V., Bobrovitskaya, N.N., 2002. A circumpolar
752 perspective on fluvial sediment flux to the Arctic ocean. *Glob. Biogeochem.*
753 *Cycles* 16, 1098. <https://doi.org/10.1029/2001GB001849>

754 Horan, K., Hilton, R.G., Dellinger, M., Tipper, E., Galy, V., Calmels, D., Selby, D.,
755 Gaillardet, J., Ottley, C.J., Parsons, D.R., Burton, K.W., 2019. Carbon dioxide
756 emissions by rock organic carbon oxidation and the net geochemical carbon
757 budget of the Mackenzie River Basin. *Am. J. Sci.* 319, 473–499.
758 <https://doi.org/10.2475/06.2019.02>

759 Huh, Y., Birck, J.-L., Allègre, C.J., 2004. Osmium isotope geochemistry in the
760 Mackenzie River basin. *Earth Planet. Sci. Lett.* 222, 115–129.
761 <https://doi.org/10.1016/j.epsl.2004.02.026>

762 Ingri, J., Widerlund, A., Land, M., Gustafsson, Ö., Andersson, P., Öhlander, B., 2000.
763 Temporal variations in the fractionation of the rare earth elements in a boreal
764 river; the role of colloidal particles. *Chem. Geol.* 166, 23–45.
765 [https://doi.org/10.1016/S0009-2541\(99\)00178-3](https://doi.org/10.1016/S0009-2541(99)00178-3)

766 Jacobsen, S.B., Wasserburg, G.J., 1980. Sm-Nd isotopic evolution of chondrites.
767 Earth Planet. Sci. Lett. 50, 139–155. <https://doi.org/10.1016/0012->
768 821X(80)90125-9

769 Jang, K., Bayon, G., Han, Y., Joo, Y.J., Kim, Ji-Hoon, Ryu, J.-S., Woo, J., Forwick,
770 M., Szczuciński, W., Kim, Jung-Hyun, Nam, S.-I., 2020. Neodymium isotope
771 constraints on chemical weathering and past glacial activity in Svalbard. Earth
772 Planet. Sci. Lett. 542, 116319. <https://doi.org/10.1016/j.epsl.2020.116319>

773 Jeandel, C., Arsouze, T., Lacan, F., Téchiné, P., Dutay, J.-C., 2007. Isotopic Nd
774 compositions and concentrations of the lithogenic inputs into the ocean: A
775 compilation, with an emphasis on the margins. Chem. Geol. 239, 156–164.
776 <https://doi.org/10.1016/j.chemgeo.2006.11.013>

777 Jeandel, C., Oelkers, E.H., 2015. The influence of terrigenous particulate material
778 dissolution on ocean chemistry and global element cycles. Chem. Geol. 395,
779 50–66. <https://doi.org/10.1016/j.chemgeo.2014.12.001>

780 Jones, M.T., Pearce, C.R., Oelkers, E.H., 2012. An experimental study of the
781 interaction of basaltic riverine particulate material and seawater. Geochim.
782 Cosmochim. Acta 77, 108–120. <https://doi.org/10.1016/j.gca.2011.10.044>

783 Köhler, S.J., Harouiya, N., Chaïrat, C., Oelkers, E.H., 2005. Experimental studies of
784 REE fractionation during water–mineral interactions: REE release rates during
785 apatite dissolution from pH 2.8 to 9.2. Chem. Geol. 222, 168–182.
786 <https://doi.org/10.1016/j.chemgeo.2005.07.011>

787 Lacan, F., Tachikawa, K., Jeandel, C., 2012. Neodymium isotopic composition of the
788 oceans: A compilation of seawater data. Chem. Geol. 300–301, 177–184.
789 <https://doi.org/10.1016/j.chemgeo.2012.01.019>

790 Leybourne, M.I., Johannesson, K.H., 2008. Rare earth elements (REE) and yttrium
791 in stream waters, stream sediments, and Fe–Mn oxyhydroxides:
792 Fractionation, speciation, and controls over REE+Y patterns in the surface
793 environment. *Geochim. Cosmochim. Acta* 72, 5962–5983.
794 <https://doi.org/10.1016/j.gca.2008.09.022>

795 Macdonald, R.W., Solomon, S.M., Cranston, R.E., Welch, H.E., Yunker, M.B.,
796 Gobeil, C., 1998. A sediment and organic carbon budget for the Canadian
797 Beaufort Shelf. *Mar. Geol.* 144, 255–273. [https://doi.org/10.1016/S0025-](https://doi.org/10.1016/S0025-3227(97)00106-0)
798 [3227\(97\)00106-0](https://doi.org/10.1016/S0025-3227(97)00106-0)

799 Martin, E.E., Blair, S.W., Kamenov, G.D., Scher, H.D., Bourbon, E., Basak, C.,
800 Newkirk, D.N., 2010. Extraction of Nd isotopes from bulk deep sea sediments
801 for paleoceanographic studies on Cenozoic time scales. *Chem. Geol.* 269,
802 414–431. <https://doi.org/10.1016/j.chemgeo.2009.10.016>

803 Martin, J.H., 1990. Glacial-interglacial CO₂ change: The Iron Hypothesis.
804 *Paleoceanography* 5, 1–13. <https://doi.org/10.1029/PA005i001p00001>

805 Merschel, G., Bau, M., Schmidt, K., Münker, C., Dantas, E.L., 2017. Hafnium and
806 neodymium isotopes and REY distribution in the truly dissolved,
807 nanoparticulate/colloidal and suspended loads of rivers in the Amazon Basin,
808 Brazil. *Geochim. Cosmochim. Acta* 213, 383–399.
809 <https://doi.org/10.1016/j.gca.2017.07.006>

810 Millot, R., Gaillardet, J. érôme, Dupré, B., Allègre, C.J., 2003. Northern latitude
811 chemical weathering rates: clues from the Mackenzie River Basin, Canada.
812 *Geochim. Cosmochim. Acta* 67, 1305–1329. [https://doi.org/10.1016/S0016-](https://doi.org/10.1016/S0016-7037(02)01207-3)
813 [7037\(02\)01207-3](https://doi.org/10.1016/S0016-7037(02)01207-3)

814 O'Regan, M., Coxall, H., Hill, P., Hilton, R., Muschitiello, F., Swärd, H., 2018. Early
815 Holocene sea level in the Canadian Beaufort Sea constrained by radiocarbon
816 dates from a deep borehole in the Mackenzie Trough, Arctic Canada. *Boreas*
817 47, 1102–1117. <https://doi.org/10.1111/bor.12335>

818 Porcelli, D., Andersson, P.S., Baskaran, M., Frank, M., Björk, G., Semiletov, I., 2009.
819 The distribution of neodymium isotopes in Arctic Ocean basins. *Geochim.*
820 *Cosmochim. Acta* 73, 2645–2659. <https://doi.org/10.1016/j.gca.2008.11.046>

821 Pourmand, A., Dauphas, N., Ireland, T.J., 2012. A novel extraction chromatography
822 and MC-ICP-MS technique for rapid analysis of REE, Sc and Y: Revising CI-
823 chondrite and Post-Archean Australian Shale (PAAS) abundances. *Chem.*
824 *Geol.* 291, 38–54. <https://doi.org/10.1016/j.chemgeo.2011.08.011>

825 Raiswell, R., Plant, J., 1980. The incorporation of trace elements into pyrite during
826 diagenesis of black shales, Yorkshire, England. *Econ. Geol.* 75, 684–699.
827 <https://doi.org/10.2113/gsecongeo.75.5.684>

828 Rickli, J., Hindshaw, R.S., Leuthold, J., Wadham, J.L., Burton, K.W., Vance, D.,
829 2017. Impact of glacial activity on the weathering of Hf isotopes –
830 Observations from Southwest Greenland. *Geochim. Cosmochim. Acta* 215,
831 295–316. <https://doi.org/10.1016/j.gca.2017.08.005>

832 Schwab, M.S., Hilton, R.G., Raymond, P.A., Haghipour, N., Amos, E., Tank, S.E.,
833 Holmes, R.M., Tipper, E.T., Eglinton, T.I., 2020. An Abrupt Aging of Dissolved
834 Organic Carbon in Large Arctic Rivers. *Geophys. Res. Lett.* 47,
835 e2020GL088823. <https://doi.org/10.1029/2020GL088823>

836 Tachikawa, K., Piotrowski, A.M., Bayon, G., 2014. Neodymium associated with
837 foraminiferal carbonate as a recorder of seawater isotopic signatures. *Quat.*
838 *Sci. Rev.* 88, 1–13. <https://doi.org/10.1016/j.quascirev.2013.12.027>

839 Tanaka, T., Togashi, S., Kamioka, H., Amakawa, H., Kagami, H., Hamamoto, T.,
840 Yuhara, M., Orihashi, Y., Yoneda, S., Shimizu, H., Kunimaru, T., Takahashi,
841 K., Yanagi, T., Nakano, T., Fujimaki, H., Shinjo, R., Asahara, Y., Tanimizu, M.,
842 Dragusanu, C., 2000. JNdi-1: a neodymium isotopic reference in consistency
843 with LaJolla neodymium. *Chem. Geol.* 168, 279–281.
844 [https://doi.org/10.1016/S0009-2541\(00\)00198-4](https://doi.org/10.1016/S0009-2541(00)00198-4)

845 Tank, S.E., Striegl, R.G., McClelland, J.W., Kokelj, S.V., 2016. Multi-decadal
846 increases in dissolved organic carbon and alkalinity flux from the Mackenzie
847 drainage basin to the Arctic Ocean. *Environ. Res. Lett.* 11, 054015.
848 <https://doi.org/10.1088/1748-9326/11/5/054015>

849 Tipper, E.T., Stevenson, E.I., Alcock, V., Knight, A.C.G., Baronas, J.J., Hilton, R.G.,
850 Bickle, M.J., Larkin, C.S., Feng, L., Relph, K.E., Hughes, G., 2021. Global
851 silicate weathering flux overestimated because of sediment–water cation
852 exchange. *Proc. Natl. Acad. Sci.* 118.
853 <https://doi.org/10.1073/pnas.2016430118>

854 Vincent, E., Berger, W.H., 1985. Carbon Dioxide and Polar Cooling in the Miocene:
855 The Monterey Hypothesis, in: *The Carbon Cycle and Atmospheric CO₂:
856 Natural Variations Archean to Present*. American Geophysical Union (AGU),
857 pp. 455–468. <https://doi.org/10.1029/GM032p0455>

858 Vonk, J.E., Giosan, L., Blusztajn, J., Montlucon, D., Graf Pannatier, E., McIntyre, C.,
859 Wacker, L., Macdonald, R.W., Yunker, M.B., Eglinton, T.I., 2015. Spatial
860 variations in geochemical characteristics of the modern Mackenzie Delta
861 sedimentary system. *Geochim. Cosmochim. Acta* 171, 100–120.
862 <https://doi.org/10.1016/j.gca.2015.08.005>

863 Vonk, J.E., Tank, S.E., Walvoord, M.A., 2019. Integrating hydrology and
864 biogeochemistry across frozen landscapes. *Nat. Commun.* 10, 5377.
865 <https://doi.org/10.1038/s41467-019-13361-5>

866 Walker, J.C.G., Hays, P.B., Kasting, J.F., 1981. A negative feedback mechanism for
867 the long-term stabilization of Earth's surface temperature. *J. Geophys. Res.*
868 *Oceans* 86, 9776–9782. <https://doi.org/10.1029/JC086iC10p09776>

869 Wheeler, J.O., Hoffman, P.F., Card, K.D., Davidson, A., Sanford, B.V., Okulitch,
870 A.V., Roest, W.R., 1996. Geological map of Canada / Carte géologique du
871 Canada. *Geol. Surv. Can. Nat. Resour. Can.* <https://doi.org/10.4095/208175>

872 Zimmermann, B., Porcelli, D., Frank, M., Andersson, P.S., Baskaran, M., Lee, D.-C.,
873 Halliday, A.N., 2009. Hafnium isotopes in Arctic Ocean water. *Geochim.*
874 *Cosmochim. Acta* 73, 3218–3233. <https://doi.org/10.1016/j.gca.2009.02.028>

875 Zolkos, S., Tank, S.E., Kokelj, S.V., 2018. Mineral Weathering and the Permafrost
876 Carbon-Climate Feedback. *Geophys. Res. Lett.* 45, 9623–9632.
877 <https://doi.org/10.1029/2018GL078748>

878

879

880

881

882 **Figure Captions**

883

884 **Figure 1.** Area of study **A.** Sample locations and elevation (GDEM, resolution 30 Arc
885 second). **B.** Bedrock geology of the Mackenzie Basin (shaded black line),
886 categorized by rock type (Wheeler et al., 1996). White circles indicate the location of
887 sampling sites identified in A.

888

889 **Figure 2.** Water discharge from the Mackenzie River (2017 and 2018). Daily
890 discharge (lines) from Environment Canada gauging station at Tsiigehtchic, retrieved
891 from the ArcticGro database (<https://www.arcticrivers.org/data>, Supplementary text
892 S2). ADCP Discharge at the Middle Channel and Tsiigehtchic (this study, light blue,
893 2017, dark blue 2018).

894

895 **Figure 3.** ϵNd on coupled HH leachates (circles), dissolved ($<0.2\mu\text{m}$ only shown)
896 and silicate residue sediment (triangles) at all sampling localities (2017 and 2018).
897 Probability density of sediment residue (green) and leachate (pink) shown, difference
898 in modes (dashed grey line) is indicated (black arrow). Open symbols are bank
899 sediment and coloured symbols, SPM, coloured diamonds are sediment core data.
900 Coloured squares are a shale fragment HH leachate and residue (pink and green
901 respectively), which was not used in the linear regression. Error bars are 2σ
902 analytical uncertainty (where visible or smaller than the symbol size). 1:1 line
903 (dashed line) is shown.

904

905 **Figure 4.** Two sediment depth profiles from the Mackenzie River (Middle Channel,
906 2017). Water depth is normalised to the deepest sample. Error bars are 2σ analytical
907 uncertainty. Dissolved compositions are from waters obtained at the surface and at
908 depth.

909

910 **Figure 5.** Probability density of the fraction of a suite of elements in leachates
911 relative to the total (sum of leachates and residue). Data is from all sampling sites
912 across both years. The fraction of the HH leachate, acetic acid leachate, and the

913 sum of all leaching steps are shown. Symbols are data points that form the
914 probability distribution.

915

916 **Figure 6. Characterisation of sequential extractions A. MREE/MREE***

917 HREE/LREE cross-plot, following Martin et al., 2010, alongside a non-exhaustive
918 literature compilation (plotted for reference, Supplementary Text S2). HREE= Σ (Tm,
919 Yb, Lu) LREE= Σ (La, Pr, Nd), MREE= Σ (Gd, Tb, Dy), MREE*=(HREE+LREE)/2. All
920 concentrations are normalised to PAAS (after Pourmand et al., 2012). Foraminiferal
921 coatings and marine leachates are extractions thought to represent Fe-Mn
922 oxyhydroxides. **B.** A REE partitioning in a Mackenzie (Middle Channel, 2017) SPM
923 sequential extraction. Left hand side axis is the REE concentration, right hand side
924 axis fraction of total (sum of leachates and residue) REE concentration (bars) in
925 each phase. **C.** $^{87}\text{Sr}/^{86}\text{Sr}$ against ϵNd on Mackenzie (Middle Channel, 2017) SPM
926 sequential extractions and water ($^{87}\text{Sr}/^{86}\text{Sr}$ data point from Tipper et al., 2021). 2σ
927 analytical uncertainty is shown, unless smaller than the symbol size.

928

929 **Figure 7.** Schematic indicating the mechanisms presented herein that may lead to
930 more radiogenic ϵNd in the HH leachates of SPM and the dissolved load of the
931 Mackenzie river, when compared to the SPM silicate residue.

932

933 **Figure 8.** Probability density of calculated $f_{\text{Nd,auth}}$ (equation 1) for 4 sampling sites
934 generated using Monte Carlo methods. Median value (white line) and interquartile
935 range (dashed lines) are shown. Input compositions for this calculation are listed in
936 Table S13.

937

938

939

940

941

942

943

944

945

946

947

948

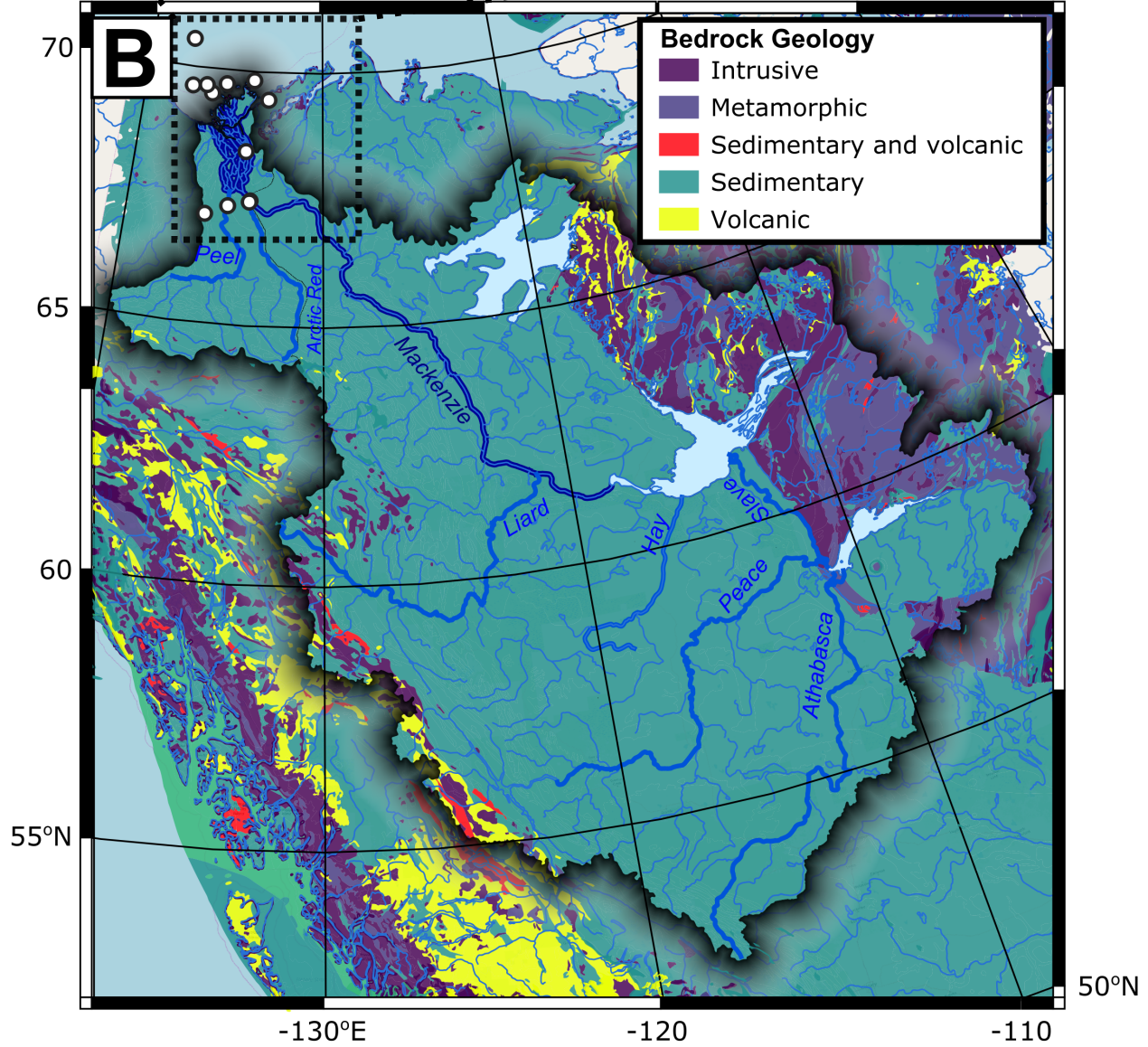
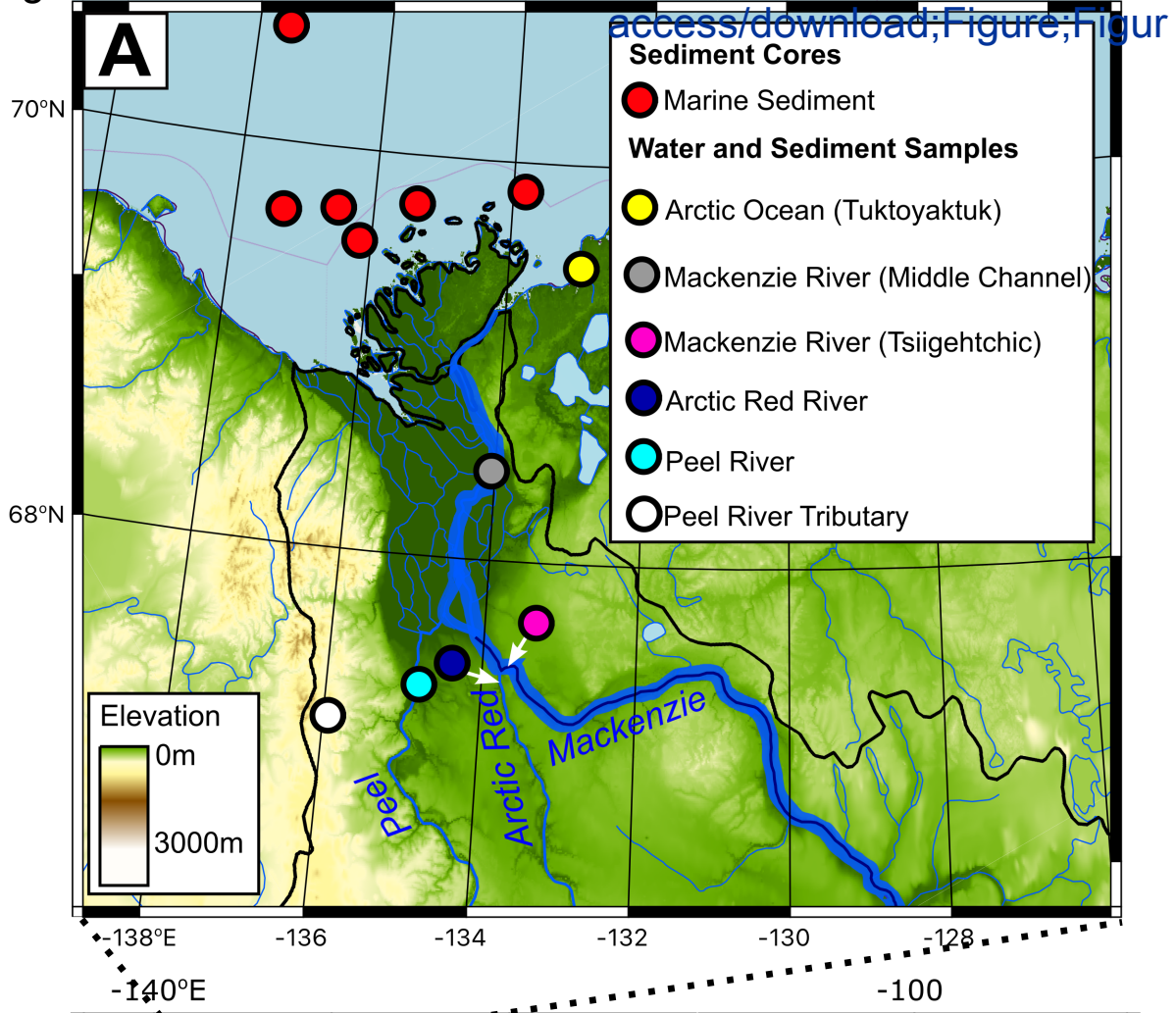
949

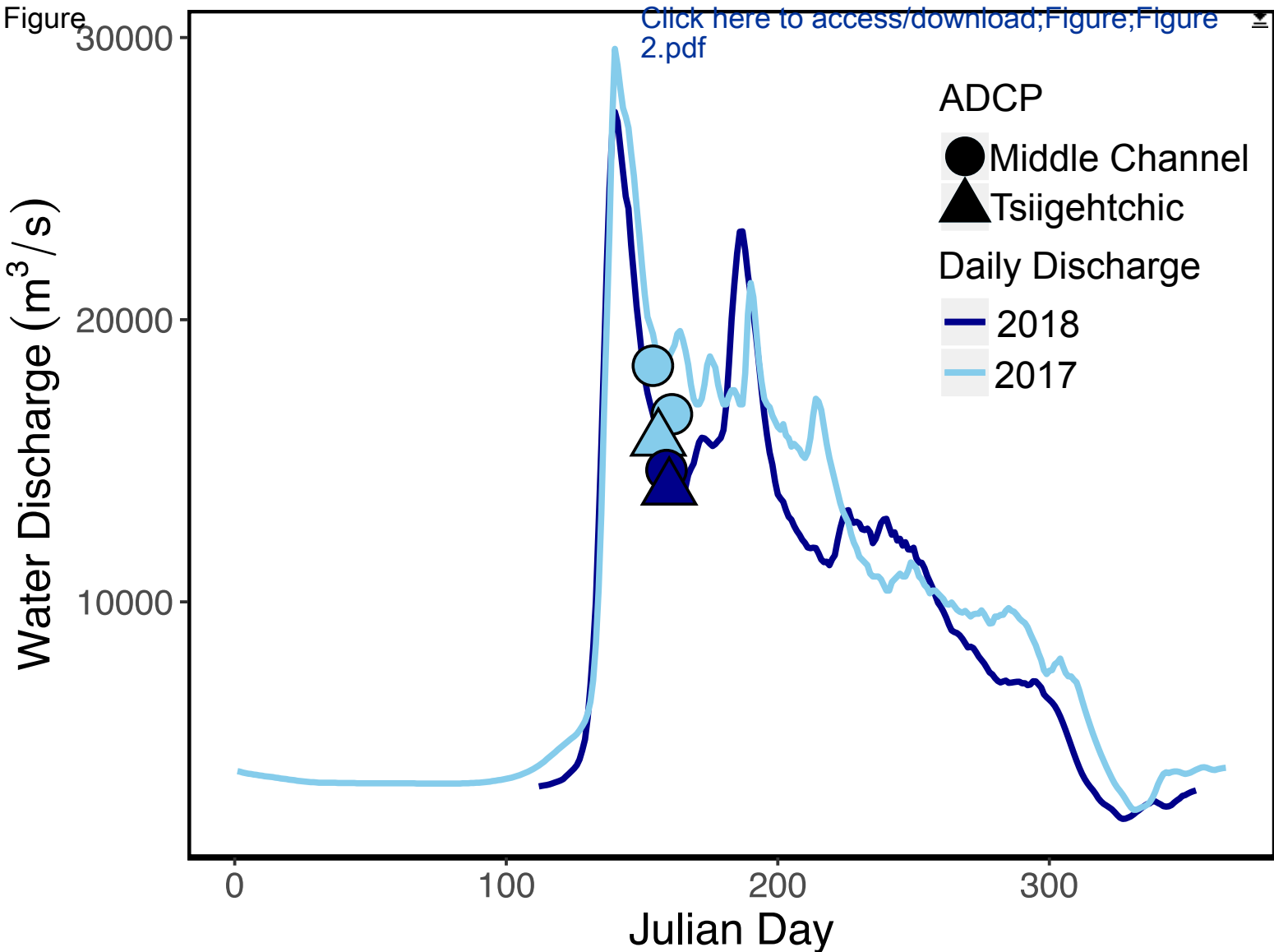
950

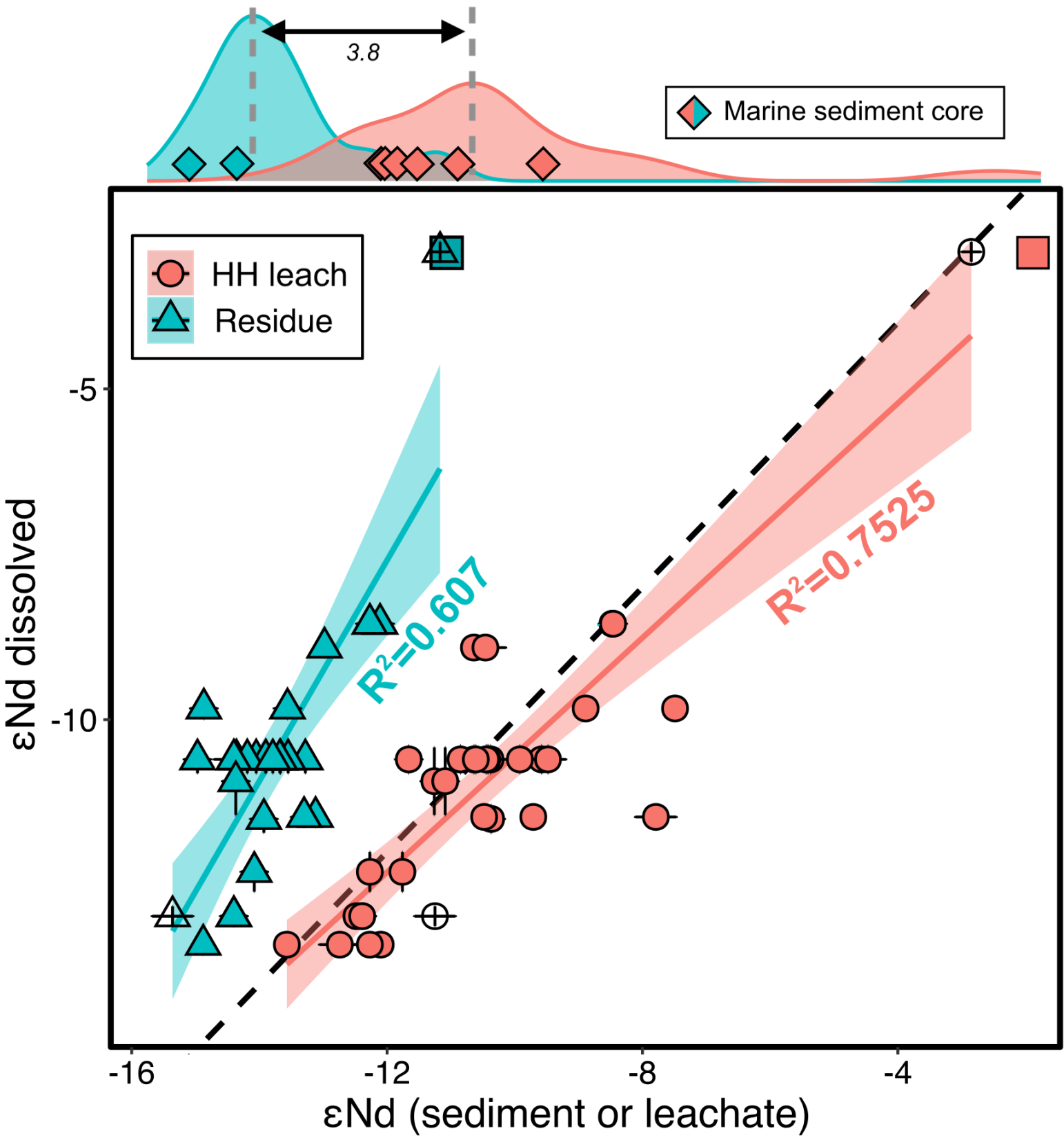
951

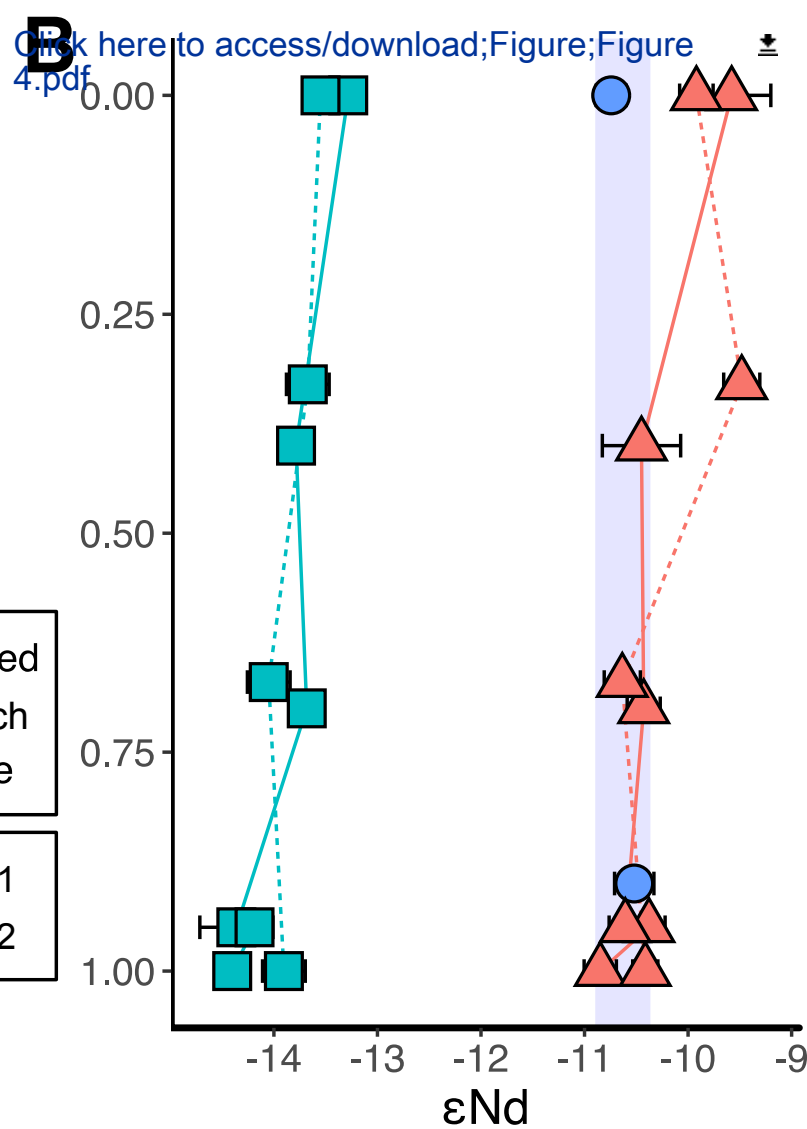
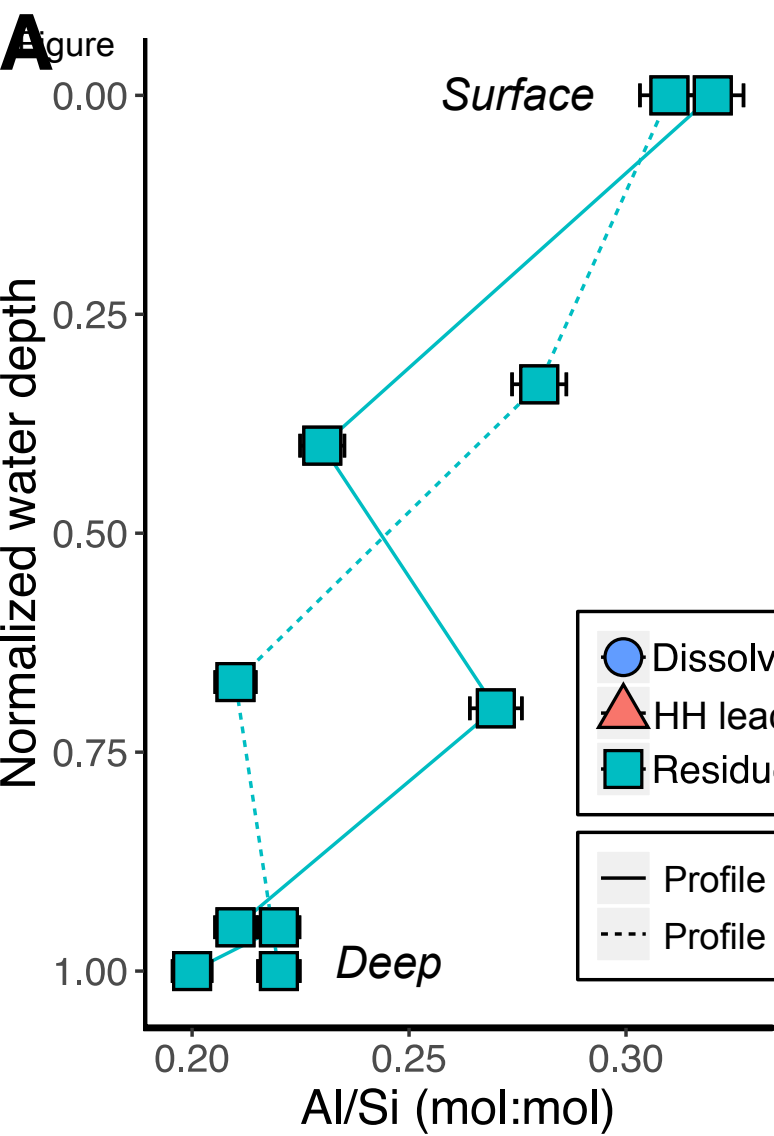
952

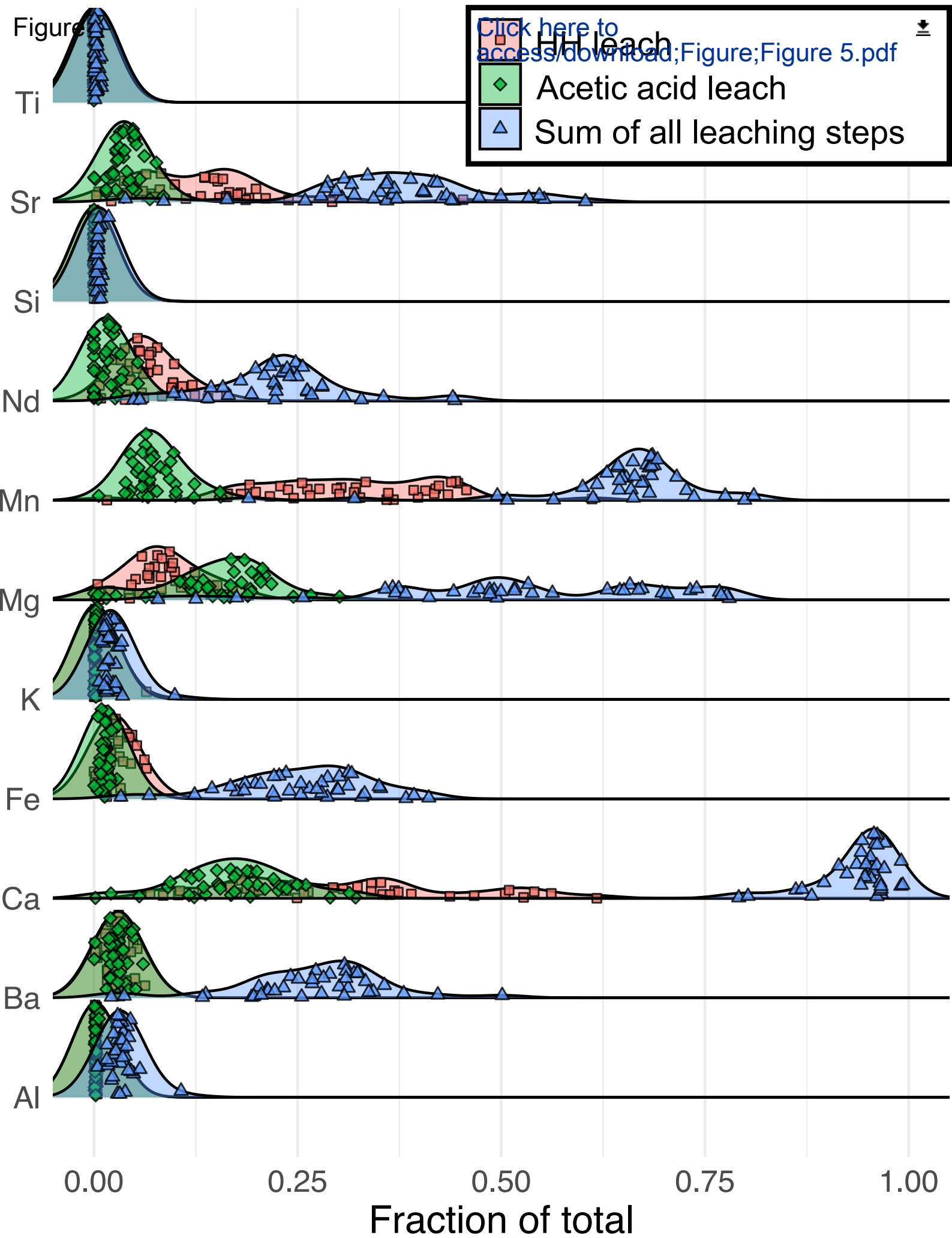
953

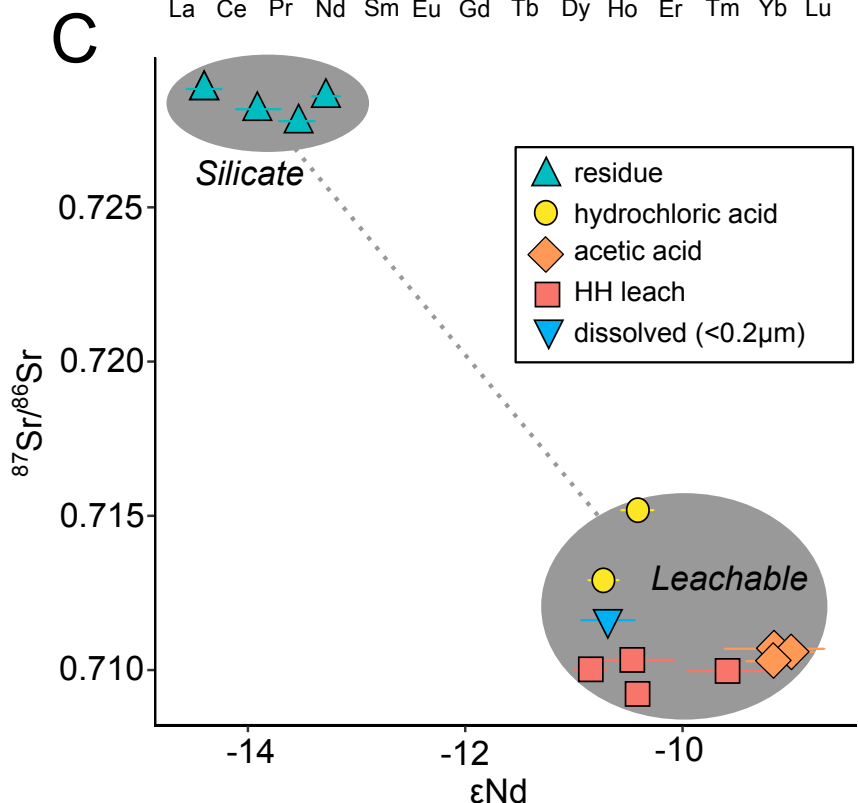
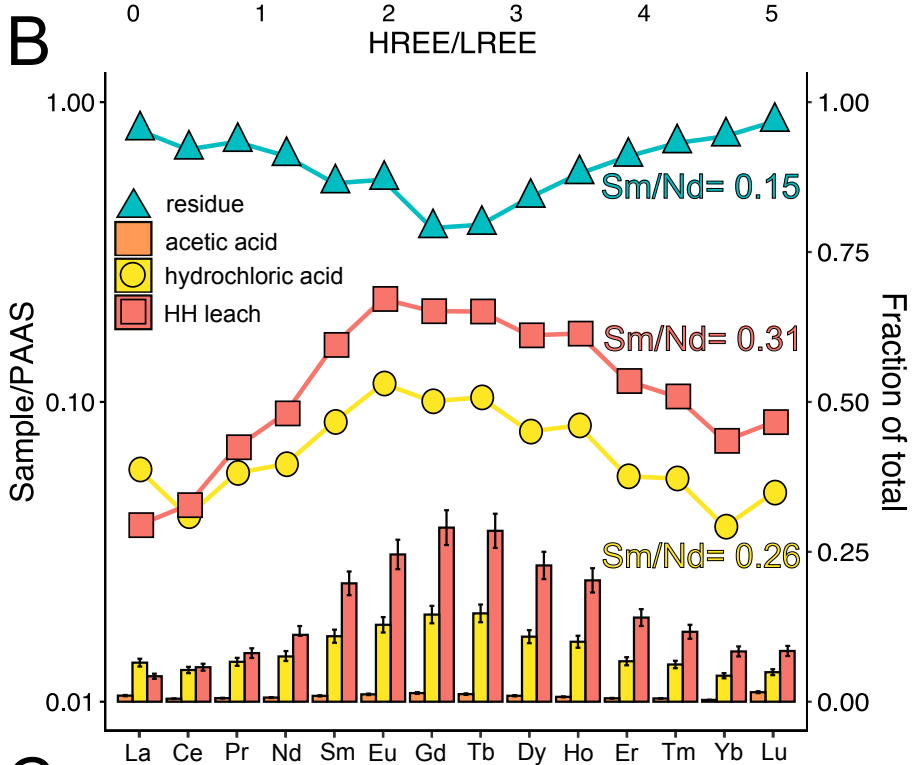
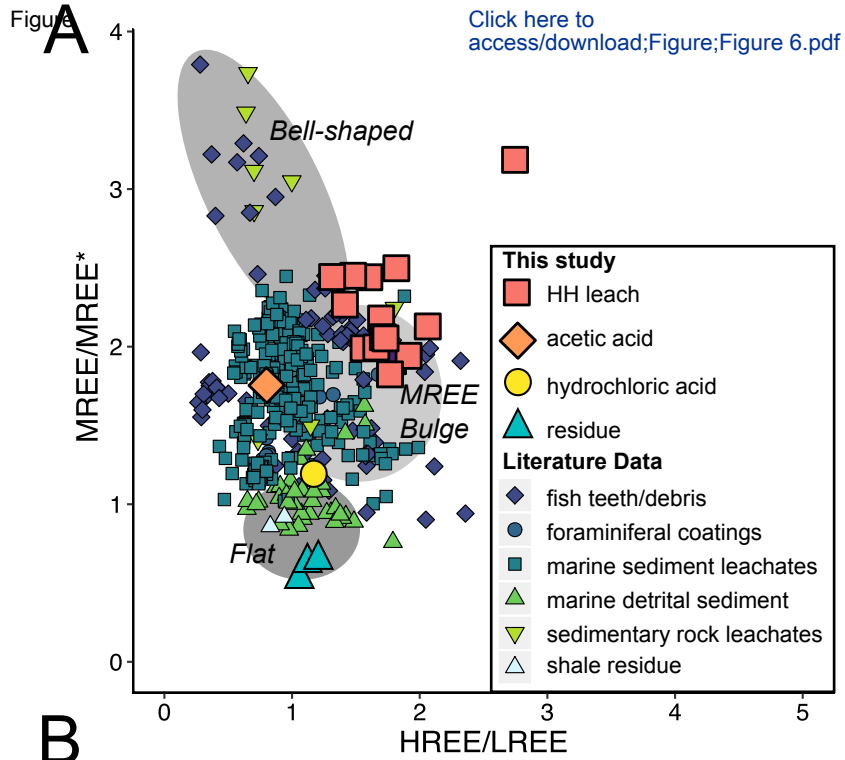






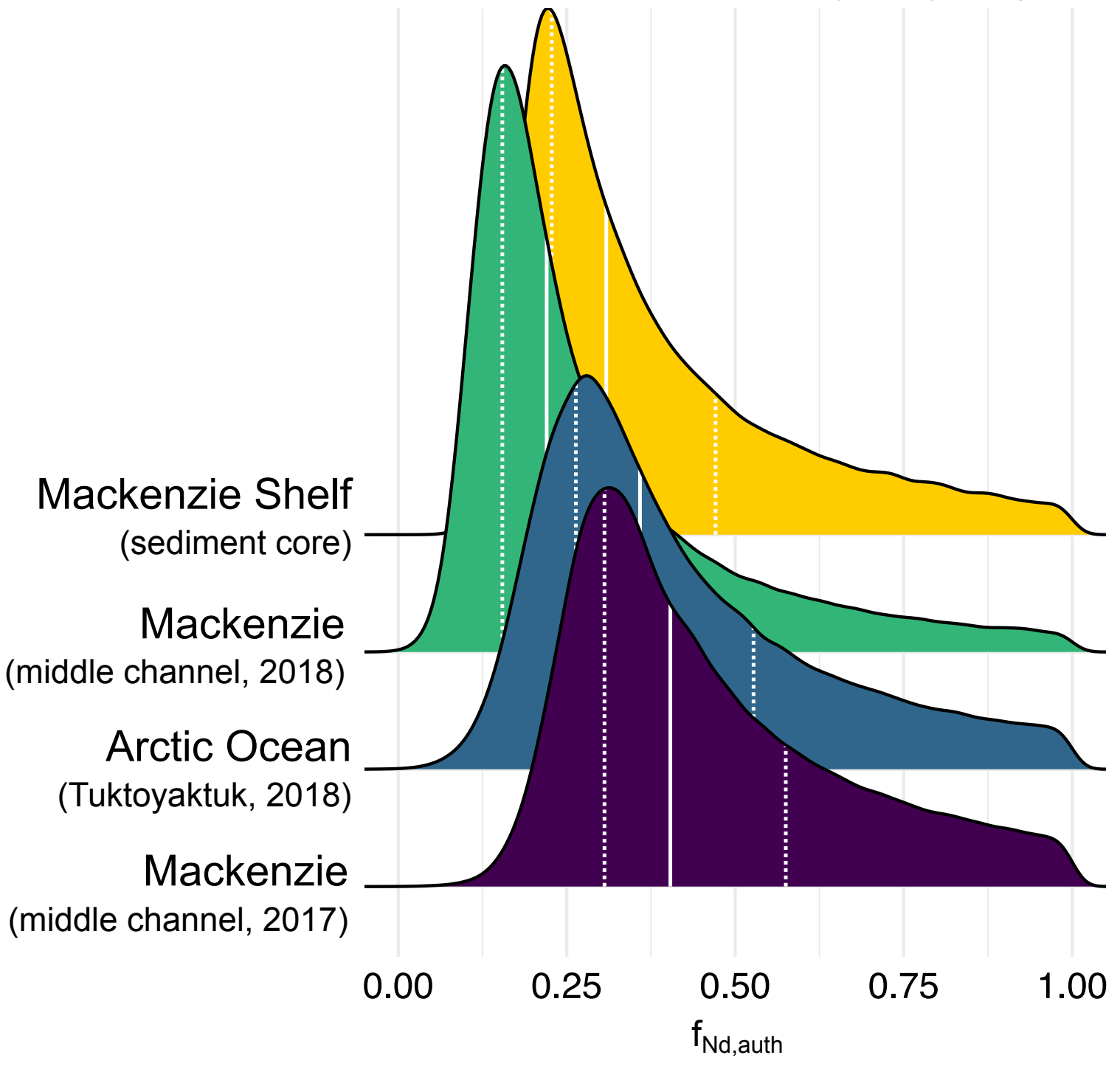






Figure

[Click here to access/download;Figure;Figure 8.pdf](#)



Sedimentary Rock

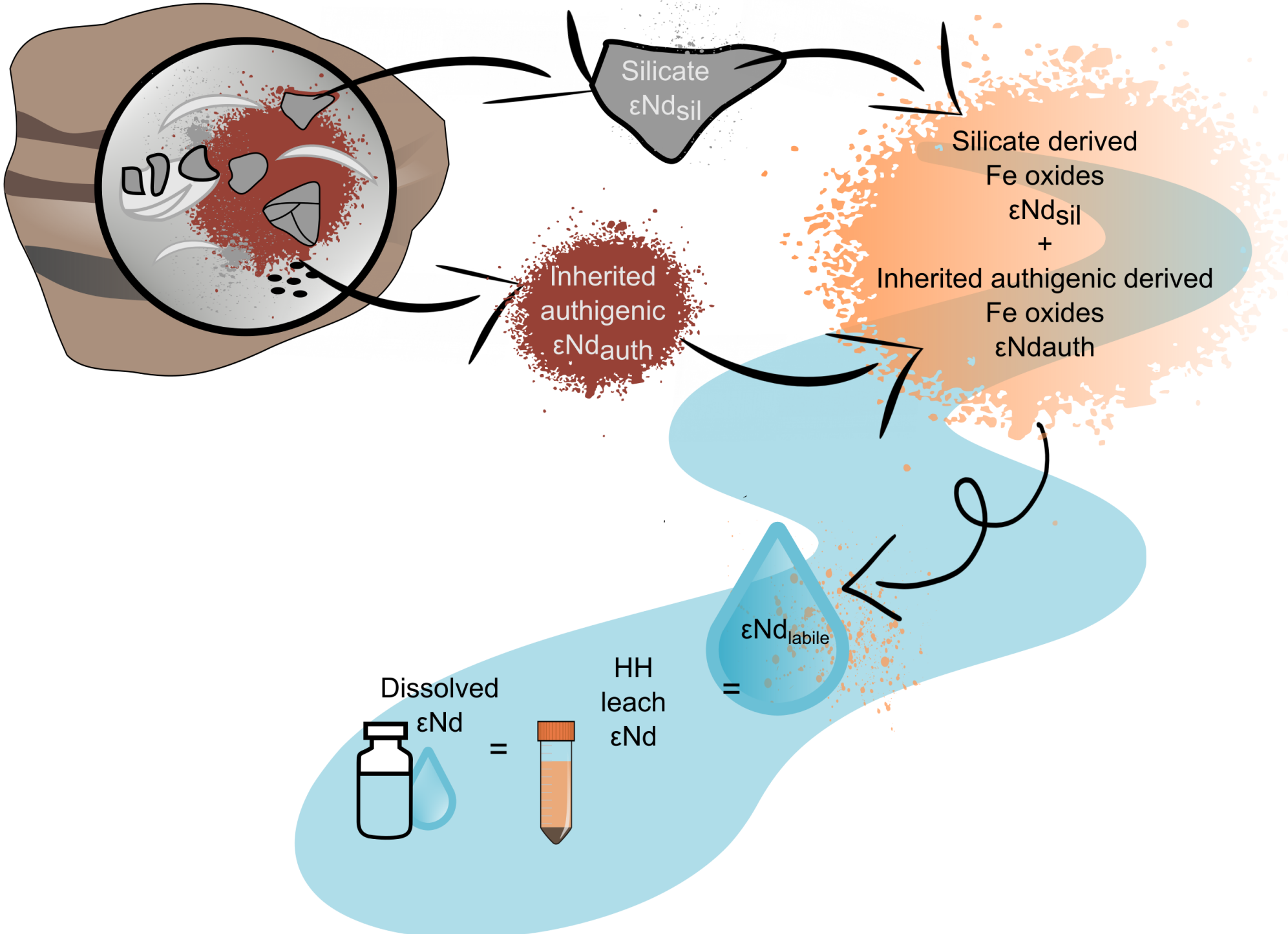


Table 1. ϵ Nd and Nd concentrations on different filtrates from the Mackenzie River and a major tributary (2018).

River	Filter Size/MWCO	ϵNd	Error (2σ)¹	[Nd] ppt	Error (2σ)	% of <0.2μm
Mackenzie River (Middle Channel)	<0.2 μ m	-12.97	0.15	20.7 ²	0.7 (n=2)	
	10kda	-12.41	0.51	10.4 ³	1.4 (n=2)	50%
	1kda	-13.40	0.34	5.9 ³	0.4 (n=2)	29%
	<0.2 μ m	-11.47	0.15	12.1	n/a (n=1)	
Peel River	10kda	-11.61	0.34	7.1 ²	0.1 (n=2)	59%
	1kda	n.d	n.d	4.1 ³	0.8 (n=2)	34%

¹Analytical uncertainty, ²Average and 2σ of two replicate measurements during different analytical sessions, ³Average and 2σ of two full procedural replicates (including filtration)

Author contributions

C.S.L, E.T.T., A.M.P, R.G.H and R.S.H designed the study. C.S.L, R.G.H, M.D, J.J.B carried out the sample collection and fieldwork. R.G.H and E.T.T and C.S.L obtained funding for fieldwork and analysis. C.S.L and R.W carried out method development to analyse the samples. C.S.L analysed the samples and wrote the manuscript under the supervision of E.T.T and A.M.P with input and guidance from all co-authors.